

POLITECNICO DI MILANO

PhD School

PhD program in Electrical Engineering
Cycle-XXIV

Dipartimento di Elettrotecnica

PROBLEMS AND SOLUTIONS IN ROTATING
MACHINES CONNECTED TO HIGH POWER DRIVES
FOR RENEWABLE ENERGY



Doctoral Dissertation of:
Daniel Felipe Ortega Belaundez
ID739068

Tutor:
Professor Dr. Francesco Castelli Dezza

The Chair of the Doctoral Program:
Professor Dr. Alberto Berizzi

February 2012

Acknowledgment

It is a pleasure to thank the many people whose contribution in assorted ways to the research, made this thesis possible.

I owe my deepest gratitude to my Ph.D. supervisor, Prof. Dr. Francesco Castelli Dezza, whose supervision, advice, guidance and from the preliminary to the concluding level enabled me to develop an understanding of the subject. As well as giving me unflinching encouragement and support in various ways.

I also appreciate insightful discussions and help on different ways to Dr. Stefania Carmelli and Prof. Dr. Gabrio Superti Furga, for all the advice and necessary theoretical concepts during unforgivable classes during the research.

Many thanks go in particular to Prof. Dr. Wajiha Shireen for her valuable advice, supervision and technical support during the stay on her laboratory of Power Electronics at University of Houston. I am much indebted to her for her invaluable help on tracking the writing of this dissertation.

I would also acknowledge to Mr. Gabriele Marchegiani for his contribution to lend very delicate equipment and rotating machines at ELVI S.p.a. company in Delebio, Italy.

Our work greatly improved thanks to the comments of the anonymous reviewers and editors of the articles published on IEEE with contributions of this dissertation.

I also thank other people I met in University of Houston for the wonderful friendship they offered me, during my stay developing important research for this dissertation like Adarsh Nagarajan and Peetham Goli. I would like to thank to my colleague Matteo Maglio, for his collaboration. I am grateful to Daniel Orellana and Leonardo Roses for their friendship and support.

Thanks also to my family, especially my mother Catalina Belaunde, to my father Miguel A. Ortega and brothers for all the love and support in all ways they always give to me during all those years during my education.

Last but not least, a special thanks to my wife, Claudia Huichalaf. Without her encouragement it would have been certainly much harder to finish a PhD. Learning to love her and to receive her love makes me a better human being.

INTRODUCTION.....	1
SYMBOLS DEFINITION	5
ABBREVIATIONS.....	7
CHAPTER I: PHENOMENA	9
1.1 Overvoltage Causes	9
1.1.1 Reflected Waves	10
1.1.2 Length of Cable and Rise Time.....	10
1.2 Partial Discharges.....	14
1.2.1 PD Pulse Coupling and Detection Devices	15
1.2.2 Display Methods	16
CHAPTER II: STANDARDS	17
2.1 National Electrical Manufacturers Association Standards NEMA MG-1 Part 30	18
2.2 National Electrical Manufacturers Association Standards NEMA MG-1 Part 31	19
2.3 International Electrotechnical Commission Standards IEC 60034-18-41	21
2.3.1 Partial Discharge and Insulation.....	22
2.3.2 Partial Discharge measurements.....	23
2.4 International Electrotechnical Commission IEC Technical Specification 61934.....	24
2.4.1 Measurements of PD under short rise time and repetitive voltage impulses	24
2.4.2 Testing conditions	25
2.4.3 PD detection methods.....	25
2.4.4 PD sensors	26
CHAPTER III: MODELS	29
3.1 Description of Universal AC Rotating Machine Model.....	29

3.2 Description of Cable Model	32
3.2.1 Impedance Measurement Technique for Cables.....	33
3.2.2 Finite Element Analysis Simulation	35
3.2.3 Comparison between Measurements and Finite Element Results	37
CHAPTER IV: FILTERS	41
4.1 Description of First Order RC Filter at Motor Terminals.....	42
4.1.1 Design of RC Filter	44
4.2 Description of Second Order RLC Filter at Inverter Terminals.....	45
4.2.1 Design of LRC Filter.....	46
CHAPTER V: CASE STUDY 1. REDUCTION OF MOTOR OVERVOLTAGE FED BY PWM AC DRIVES USING A UNIVERSAL MODEL.....	49
5.1 Introduction	50
5.2 Analysis of Components.....	51
5.2.1 Three Phase Cable for PWM AC Drives.....	51
5.2.2 Application of First Order RC Filter at Motor Terminals	52
5.3 Measurements Results.....	53
5.4 Determination of Motor Parameters.....	55
5.5 Simulations Results.....	57
5.6 Validation of Motor Model	62
5.7 Conclusions	63
CHAPTER VI: CASE STUDY 2. ON LINE PARTIAL DISCHARGES TEST ON ROTATING MACHINES SUPPLIED BY IFDS	65
6.1 Introduction	66
6.2 Simulation Components.....	68
6.2.1 Application of Cable Model	68
6.2.2 Used Rotating Machine Model.....	69
6.3 On line PD Test Components.....	70
6.3.1 General	70

6.3.2 Settings	70
6.4 Simulation Results	71
6.5 Conclusions	76
CHAPTER VII: BACK TO BACK CONVERTER	79
7.1 Inverter Control.....	79
7.1.2 Three Phase Grid Side Converter Control.....	79
7.1.3 Single Phase Grid Side Converter Control.....	81
7.2 Stator Side Converter Control.....	82
CHAPTER VIII: CASE STUDY 3. CONTROL FOR GRID CONNECTED PMSG WIND TURBINE WITH DC LINK CAPACITANCE REDUCTION	85
8.2 Parameters of Permanent Magnets Synchronous Machine	87
8.3 New Implementation of Algorithm on Wind Energy	88
8.3.1 The proposed Solution.....	88
8.3.2 Demonstration	89
8.4 Simulations Results.....	91
8.4.1 Connection to Three Phase Grid.....	92
8.4.2 Connection to Single Phase Grid.....	95
8.5 Conclusion	97
IX. FINAL CONSIDERATIONS.....	99
X. APPENDIX	105
10.1 Appendix A Parameters of Case Study 3.....	105
10.2 Appendix B Clark and Park Transform.....	107
10.2.1 Clark Transform	108
10.2.2 Park Transform.....	108
10.2.3 Inverse Park and Clarke Transform.....	109
10.2.4 Summary	109
10.2.5 Single Phase d-q Transformation	110

XI. REFERENCES 111

Introduction

This thesis investigates the related problems when rotating machines are connected to power converters and their solutions. The topics developed are:

- Reduction of overvoltage on terminals and windings of Induction Motor (IM) fed by Adjustable Speed Drives (ASD).
- Online Partial Discharges (PD) test on windings of Induction Motor fed by Adjustable Speed Drives, with reduction of Partial Discharge Inception Voltage (PDIV).
- Protection against noise in Torque and Currents of Permanent Magnet Synchronous Generator (PMSG) for Wind Energy Conversion System (WECS), connected to a Back to Back converter, with a DC-Link capacitance reduction.

Industrial applications of adjustable speed drives using Pulse Width Modulated (PWM) voltage source inverters with steep voltage pulse rise time has evolved and are more sophisticated, having faster rise time ($<100\text{ns}$) allowing higher control bandwidth and reducing inverter switching losses, and faster switching cycles (4-20kHz) to reduce motor current ripple harmonics, and acoustical noise improving the system behavior. However, the rise time of the voltage transition also excites undesirable secondary effects, such as reflected wave spikes on motor terminal that rise the aging of the insulation in the machine. With a square wave from PWM from inverter could produce motor transients up to twice the dc-bus voltage due to mismatch between the cable impedance and the machine surge impedance, thus creating the reflected wave. The length of conductor between machine and inverter may be critical since could be the reason of twice voltage magnitude, also depends on pulse rise time. In the state of art of Insulated Gate Bipolar Transistor (IGBT) rise time depends on the active power, and considering the situation that could be around of $tr = 0.05\mu\text{s}$, the critical cable length could be 15m (50ft). When the rise time of IGBT is faster; a nonlinear voltage gradient on the first coil of the machine winding is created [1]-[2]. The Over-voltages on terminal of machines and windings can lead to inter-turn short circuit failure and phase to phase or phase to ground faults [3]. The fast rise time can create significant issues besides of over-voltage on terminal machines such as communications interference, and bearing currents [4]-[5]-[6]-[7]. The analysis of these phenomena is presented on Case Study 1

Chapter VI, where all the theory found on bibliography is practical verified. Simulations, experimental results on University laboratory and machine measurements performed with a RLC bridge on workshop of ELVI Spa Company, are obtained in order to construct and verify an innovative Universal Induction Machine Model. The IM model is Universal in the sense that Common Mode (CM) and Differential Mode (DM) are placed together into one three-phase equivalent circuit model. The effect of length of cable is also experimentally verified on laboratory using a scale system of 1.1kW Induction Motor connected through a 7.7 meters long cable between Induction Motor and the output of the inverter. On simulations it is verified a simple solution for overvoltage reduction using a First Order RC Low Pass Filter on Terminal of IM. The author of this thesis has presented this research on Case Study 1 in paper [8] to IEEE ICEM 2010 Conference and it is currently on review for IEEE-IAS Journal.

An on line Partial Discharge test technique on Induction Motor fed by an inverter and a reduction of Partial Discharge Inception Voltage (PDIV) are accomplished on Case Study 2. The Partial Discharge Inception Voltage is by definition, the lowest voltage at which Partial discharge occurs, continuously, above some stated magnitude [9]-[10]. Partial Discharge (PD) in high voltage is unfavorable to the long term operation and is associated with insulation failure. The measurements system operating within 1-20 MHz range with multiple PD sensors distributed throughout the object, can evade PD attenuation problem while localizing the PD activity. The PD sensor can be coupling capacitors and radio frequency current transformers; in our case coupling capacitors are used. Continuous monitoring system and remote communications could access and store information for further analysis by PD experts. When motors with high PD activity are connected to a bus and switched on and off, those components can produce changes that can be interpreted wrongly by periodical testing and result in wrong maintenance decisions. Continuous monitoring also excludes human induced error in the measurement process. The real operating conditions are reflected in continuous PD data trend revealing the entire history of the Induction Motor [11]. Partial Discharge activity on rotating machines connected to converters is related to overvoltage on terminals and windings due to the reflected waves from Insulated Gate Bipolar Transistor that becomes on spikes, incremented by length of cable and rise time t_r of Pulse With Modulation [12]-[13]-[14]. The simulation components to set the On Line Partial Discharge measurement were selected, such as Coupling Capacitor and High Pass Filter, and the connected Induction

Motor model is 100HP. On Case Study 2 Partial Discharge is not simulated but the Partial Discharge Inception Voltage. After the acquisition of PDIV activity on the Induction Motor, a Second Order Inverter Output RLC Low Pass Filter was placed, in order to accomplish attenuation of Partial Discharge Inception Voltage, simulations results of Case Study 2 are in Chapter V. The author of this thesis has presented the paper [12] regarding this Case Study 2 in IEEE ICEM 2010 Conference.

On the development of this thesis an algorithm is used for first time on Back to Back converter. The algorithm is placed on Grid Side Converter (GSC) when a DC-Link capacitance is reduced, protecting Permanent Magnet Synchronous Generator (PMSG) from low frequency noise from grid. The main aim of this work is to protect the PMSG from losses due to harmonics and ensure reliability of system generation by reducing the DC-Link capacitance. The Chapter VIII: Case Study 3 addresses modeling and control of the Back to Back converter and multi-pole PMSG to be used with a wind turbine. This variable speed wind turbine concept is without pitch control and this application is oriented to be connected to single phase or three phase grid. With fewer components it requires low maintenance, reduced losses and cost and at the same time has high efficiency and good controllability. The capacitance reduction through the use of the algorithm can be used on three phase grid connection and in a single phase grid connection as well. Simulation results has been shown that DC-Link voltage behavior is the same of large capacitor, compared with algorithm implemented and small DC-Link capacitor. The correction of DC-Link voltage after capacitance reduction, allows to the system to reduce the low frequency harmonics that affected the torque and currents in PMSG used in this Wind Energy Conversion System, thus protecting the machine from losses; one of the principal aim of this thesis.

In our grid connected operation, when power from PMSG is less than power available on grid, the Grid Side Converter is used to regulate the DC-Link voltage and the GSC is used to regulate the reactive power on the grid connection where should be equal to zero. For controlling the PMSG is necessary to know the rotor position and speed. They are known by using a position or speed sensor. The PMSG is magnetized from permanent magnets placed on the rotor instead using a DC excitation circuit. Thus the electrical losses of the machine are reduced and the absence of the field losses improves the thermal characteristics of the permanents magnets machines. With no mechanical components such as slip rings and brushes the is generator lighter, having a high power to weight ratio: this means a higher efficiency and reliability [15]; adding to those characteristics of machine the new capacitance

reduction and protection of this machine from losses, an innovative, efficient and reliable system is developed as the last case study on this thesis. The author of this thesis sent the paper [16] regarding to this Case Study 3 to an IEEE-PES Conference.

Symbols Definition

t	Time
t_r	Rise Time
τ	Pulse Width
ψ_{pm}	Flux Linkage Permanent Magnets
K	Amplitude of ripple on V_{dc}
ω_r	Angular frequency of V_{dc} ripple
ω_r	Angular frequency of V_{dc} ripple
ω	Grid angular frequency
θ_g	Grid Signal theta angle
θ_s	Stator Signal theta angle
ω_e	Rotor angular speed
ε	Electromotive Force
i_β	Imaginary Component Orthogonal Reference Frame
i_α	Real Component Orthogonal Reference Frame
i_0	Homopolar Component of the System
T_m	Rotor Mechanical Torque
T_e	Electromechanical Torque
L_g	Grid Side Inverter Output Inductance
L_s	Stator Inductance
R_s	Stator Resistance

i_q	Quadrature Current axis
i_d	Direct Current axis
V_q	Quadrature Voltage axis
V_d	Direct Voltage axis
V_{dc}	Voltage on DC Link without Ripple
n_{pp}	Pairs Machine poles
n_p	Machine poles
V_{cr}	Critical Voltage

Abbreviations

PD	Partial Discharge
PDIV	Partial Discharge Inception Voltage
PDEV	Partial Discharge Extinction Voltage
RPDIV	Repetitive Partial Discharge Inception Voltage
BJT	Bipolar Junction Transistors
RPDEV	Repetitive Partial Discharge Extinction Voltage
EIS	Electrical Insulation System
IM	Induction Motor
DC	Direct Current
AC	Alternate Current
CM	Common Mode
DM	Differential Mode
PWM	Pulse Width Modulation
ASD	Adjustable Speed Drives
WECS	Wind Energy Conversion System
PMSG	Permanent Magnet Synchronous Generator
IGBT	Insulated Gate Bipolar Transistor
SSC	Stator Side Converter
GSC	Grid Side Converter
FEA	Finite Element Analysis

Chapter I: Phenomena

1.1 Overvoltage Causes

This chapter presents explanations of the impact of high frequency converters over the insulation and windings of rotating machines. If pulses take longer than half rise time to travel from inverter to motor, then a full reflection will happen at the motor, thus the pulse amplitude will approximately double [17]-[18]-[19].

The Bewley diagram is a well-known graphical method which helps to determine the traveling voltage versus time, at discrete points along the cable. In order to determine the voltage at point x of the cable, this method adds all the incident and reflected waves of the voltages which cross the point x during time [20].

1.1.1 Reflected Waves

A repetitive steep wave front produced by insulated gate bipolar transistor (IGBT) drives may put the motor insulation through an accelerated aging [21]-[22]-[23]-[3]. On paper [17] author reported that an incident wave called e , which travels along a cable will behave in well-defined ways at the end of the cable, dependent upon the match or mismatch of the cable characteristic surge impedance Z as compared with the impedance closing the cable at its end R_o . If there is a mismatch, a reflection will occur, and the reflection wave is called e' . And the result of voltage at the end of cable is $eo = e + e'$.

$$e' = \frac{R_o - Z}{R_o + Z} * e \quad (1.1)$$

$$eo = \frac{2 * R_o}{R_o + Z} * e \quad (1.2)$$

Matching R_o & Z $e = 1$, $e' = 0$ and $eo = 1$

Open Circuit $e = 1$, $e' = 1$ and $eo = 2$

A positive pulse e is sent from inverter to motor. This pulse travels at speed of approximately 125-200 m/ μ s, depending upon the physical construction of the cable. When the wave reaches the motor, a reflected wave e' returns towards the inverter. At the same time at motor terminals the voltage is $eo = e + e' = 2e$. It should be noted that the voltage e , e' & eo are all ramping up to their values during the rise time Tr . The reflected wave e' reaches the inverter terminals, then a second reflection occurs and the wave starts building up towards $-2e$. This negative wave then reaches the motor and reflects back again, and so on[17].

1.1.2 Length of Cable and Rise Time

A combination of short rise time and long cable is potentially hazardous for electrical rotating machine insulation. The rise time of inverter output pulses plays a significant role in motor withstand. The rise time of the drive pulse primarily determines the critical cable length from the inverter to the motor in order to prevent overvoltage [21]. And the rise time is controlled by the Gate Turn off Thyristors (GTO) or the Insulated Gate Bipolar Transistors (IGBT) being in the order of 2-10 μ s and 50-400 ns respectively [4].

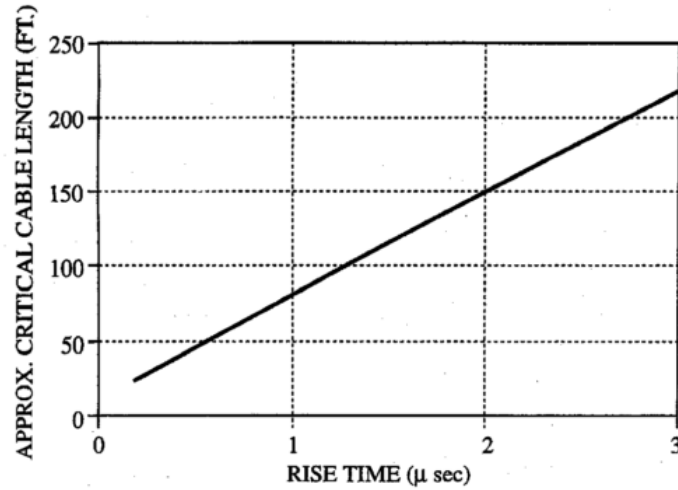


Fig.1.1 Rise Time vs. Cable Length[21]

Designers usually determine conservative cable lengths for which the peak voltage value is equal to the motor insulation class. Also critical cable length is calculated using standing wave analysis. The drive pulse risetime is controlled by the switching device risetime. Risetime is converted to an equivalent sinewave frequency and wavelength λ in meters where $c = \text{speed of light} = 3 \times 10^8 \text{ m/s}$. Equating Lc to the quarter wavelength distance $\lambda/4$, where peak standing waves of 2 p.u. are developed and substituting (1.3) into (1.4) yields the critical cable distance Lc where peak over voltage occurs [24].

$$f_e = 1/(\pi * Tr) \quad [\text{Hz}] \quad (1.3)$$

$$\lambda = c/f_e \quad [\text{m}] \quad (1.4)$$

$$Lc = 772.8 * (Tr \text{ in } \mu\text{s}) \quad [\text{Ft}] \quad (1.5)$$

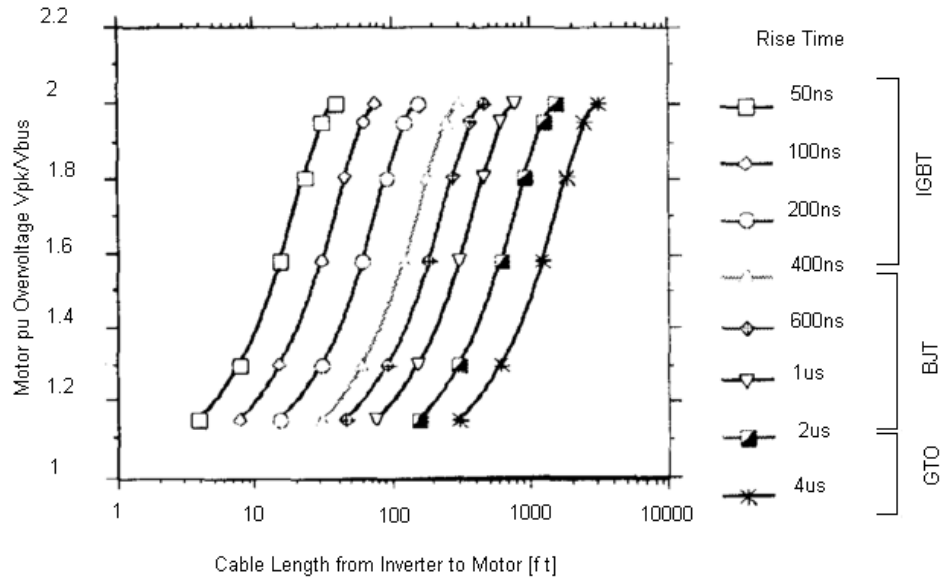


Fig. 1.2 Motor p.u. over voltage vs. cable length vs. risetime [4]

This will make possible the determination of a safe cable length which will give a peak voltage lower than the value given by equation (1.1) where V_{cr} is the critical voltage (depending on the motor insulation class); and V_{dc} is the dc bus voltage. Table 1.1 presents, for each IGBT type, the safe cable length not to be exceeded.

$$V_{pk} = \frac{V_{cr} + V_{dc}}{2} \quad (1.6)$$

The cable used on data reported on Tables 1.1 and 1.2 is (VFD TC 29501) 14 AWG, VFD 1000 V UL 4-conductors Flexible cable with a tinned copper braid shield, BELDEN Brand.

The Table 1.2 shows the critical length of cable versus IGBT rise time, their associated dc bus voltage level and maximum peak voltage levels obtained with three different cable lengths.

TABLE 1.1
SAFE CABLE LENGTH VERSUS IGBT TYPE [25]

IGBT type	DC bus voltage	Swing time (ns)	Safe cable length (ft) vs. Motor insulation class			
			A	B	C	D
400 V	300 V	50 ns	*	*	*	*
		300 ns	*	*	*	*
600 V	500 V	70 ns	15	18	*	*
		300 ns	63	78	*	*
1200 V	750 V	100 ns	15	19	22	24
		300 ns	46	56	65	73
1700 V	850 V	200 ns	14	34	40	43
		400 ns	57	68	80	87

*: The motor is relatively safe at any cable length

TABLE 1.2
PEAK VOLTAGE VERSUS IGBT TYPE AT CRITICAL CABLE LENGTH [25]

IGBT type	DC bus voltage	Swing time (ns)	Critical length ℓ_c (ft)	Peak voltage (V)		
				ℓ_c	$0.75 \ell_c$	$0.5 \ell_c$
400 V	300 V	50	13.65	566	450	315
		300	81.92	566	440	315
600 V	500 V	70	19.11	943	734	525
		300	81.92	943	734	525
1200 V	750 V	100	27.3	1415	1100	787
		300	81.92	1415	1100	787
1700 V	850 V	200	54.61	1600	1248	892
		400	109.22	1600	1248	892

1.2 Partial Discharges

This thesis states that Partial Discharges are related to overvoltages due to the rotating machine connected to converters. Now with the concept more developed, overvoltage due to the reflection wave always results in an aging of insulation. When accelerated and advanced aging is present in insulation, the risk of partial discharge is increased. In this section some definition will be reported according to references in order to analyze this phenomenon.

In reference [9] it is reported the theory analyzed on this chapter being one of the most significant approach used to develop this subject.

Partial Discharge (PD) is the electric discharge that only partially bridges the insulation between conductors. Also PD is the current or voltage pulse at the terminal of the object under test that results from a partial discharge occurring within the object under test. The Partial Discharge Inception Voltage (PDIV) is, by definition, the lowest voltage at which Partial discharge occurs, continuously, above some stated magnitude. The Partial Discharge Extinction Voltage (PDEV) is the lowest magnitude at which repetitive PD cease to occur in the test object; in practice this voltage is the lowest applied at which the magnitude of a chosen PD pulse quantity becomes equal to, or less than, a specified low value. Those pulses are measured using suitable detector circuits, which have been introduced into the test circuit for the purpose of the test.

The test object behaves predominantly as inductive, capacitive or distributed equivalent impedances according to the voltage supply frequency content. For some test objects, whether they are predominantly inductive, capacitive or distributed may depend on the PD detection frequency range. The types of test objects may include: stator and rotor windings; transformers windings; motorettes and formettes. And the capacitive test objects may include: twisted pairs of winding wire; capacitors; packing of switching devices; power electronic modules and substrates; main wall insulation models in stator coils and bars.

The PD associated quantities will depend upon specific features of the impulse waveform, for example the impulse ride time, the impulse decay time, the impulse repetition rate and the number of oscillations in the impulse. For the purpose of comparison between different insulating materials or design solutions, partial discharge measurements can be performed using standardized voltage supply waveforms. The appropriate pulse waveform can depend

on the type of test object and the type of application. The specification of the pulse supply should include, amongst other factors: pulse rise time; pulse voltage polarity; pulse repetition rate; pulse width; pulse duty cycle.

The PD can be affected by the following environmental factors: humidity; temperature; degree of contamination of the test object; atmospheric pressure and type of gas.

1.2.1 PD Pulse Coupling and Detection Devices

Partial Discharge pulses in a test object can be detected either by means of high voltage capacitors, high frequency current transformers (HFCT) or electromagnetic couplers such as antennas. The detectors, in conjunction with the rest of the measuring system, must be able to suppress the impulse voltage to a magnitude less than that expected from the PD pulse using appropriate filters.

Since the voltages impulses and PD pulses contain high frequency components, short, non-inductive earthing of the supply, the test object and the PD detector is required.

A coupling capacitor with a voltage rating exceeding the expected applied impulse voltage, together with a filter that strongly attenuates the test voltage impulses, can be used. The filter should have at least three poles and special measures to inhibit passive or active filter technology. The coupling capacitor is connected to the test object high-voltage terminal.

The HFCT with multipole filter, together with a filter, can be used to detect PD pulses while suppressing the impulse voltage. Note that HFCTs may have a very wide range of upper cut-off frequencies that may affect the performance of this method. The HFCT should have higher cut-off frequency than voltage impulse frequency. The filter should have at least three poles and special measures to inhibit cross coupling of the input signal to the output. The filter can be implemented using passive or active filtering technology. The HFCT should be placed over the high voltage cable between the impulse supply and the test object. In this case, the HFCT should have sufficient electrical insulation to ensure that breakdown between the cable and the earth. Only mains voltage insulation is then required.

1.2.2 Display Methods

The result of PD test is PDIV and PDEV. In addition, the PD pulse repetition rate and the largest peak PD pulse magnitude at a specified test voltage as well as the test conditions should be measured. It should be pointed out that PD magnitude is only a relative measure of PD activity, seeing that PD pulses are attenuated and distorted when they travel from the source to the measurement point. The PD signal output from the coupler and detection system can be recorded on a digital oscilloscope or pulse magnitude analyzer. For oscilloscope display, the PD output is normally displayed on one channel, while a reduced magnitude version of the applied impulse voltage is recorded on another channel. The magnitudes of the PD pulses as well as the temporal position in which they occur with respect to the impulse voltage are recorded.

Chapter II: Standards

The standard related to the problem of overvoltage in the rotating machines has been reported in different organization such as IEC and NEMA. In the present chapter will be analyzed those standards. The methods for measurements of the Partial Discharge Inception Voltage and overvoltage will be exposed. The information analyzed in this chapter is according to the standards reported on the titles of sections. Those standards are summarized in order to show the content related to the interests of this thesis and accomplish a comparison between them.

2.1 National Electrical Manufacturers Association Standards NEMA MG-1 Part 30

The information in this Section applies to 60 Hz NEMA Designs A and B squirrel-cage motors covered by Part 12 and to motors covered by Part 20 rated 5000 horsepower or less at 7200 volts or less, when used on a sinusoidal bus with harmonic content, or when used with adjustable-voltage or adjustable-frequency controls, or both.

Motor efficiency will be reduced when it is operated on a control. The harmonics present will increase the electrical losses, which decrease efficiency. This increase in losses will also result in an increase in motor temperature, which further reduces efficiency.

The quantitative effects of peak voltage and rise time on motor insulation can be limited. It can be assumed that when the motor is operated under normal service conditions there will be no significant reduction in service life due to voltage stress, if the following voltage limit values at the motor terminals are observed.

Motors with base rating voltage $V_{rated} \leq 600$ volts:

$$V_{peak} \leq 1kV$$

$$Rise\ time \geq 2\mu s$$

See Fig.2.1 for a typical voltage response at the motor terminals for an illustration of V_{peak} and rise time. Motors with base rating voltage $V_{rated} > 600$ volts:

$$V_{rated} \leq 2.04 * V_{rated}$$

$$Rise\ time \geq 1\mu s$$

Where:

V_{peak} is a single amplitude zero to peak line to line voltage.

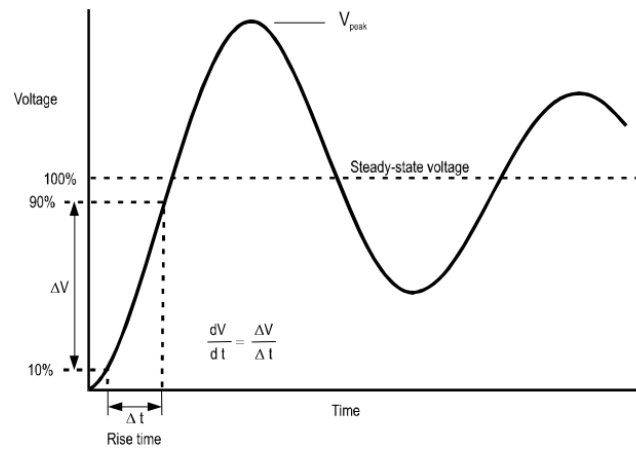


Fig. 2.1

When the input voltage to the control exceeds the rated voltage, care must be taken in determining the maximum peak voltage V_{peak} that will be applied to the motor by the control.

For suitability when values are outside these limits the manufacturer data is required. Filters, chokes, or other voltage conditioning devices, should be applied with guidance of the control manufacturer.

2.2 National Electrical Manufacturers Association Standards NEMA MG-1 Part 31

In this standard the information applies to define purpose poly-phase squirrel-cage induction motor rated 5000 horsepower or less at 7200 volts or less, intended for use with adjustable-voltage and adjustable control, such as inverters.

The conditions of additional hazard depend upon the degree of differences from usual operating conditions and the severity of the environment to which the machine is exposed. The hazard can be overheating, mechanical failure, and abnormal deterioration of the insulation system, corrosion and fire.

High frequency harmonics of inverters can cause an increase in the magnitudes of leakage currents in the motor due to a reduction in the capacitive reactance of the winding insulation at higher frequencies. Established and safe grounding practices for the motor frame should therefore be followed.

Inverters used to supply adjustable frequency power to induction motors do not produce sinusoidal output voltage waveforms. In addition to lower order harmonics, these waveforms also have superimposed on them steep-fronted, single-amplitude voltage spikes. Turn-to-turn, phase-to-phase, and ground insulation of stator windings are subjected to the resulting dielectric stresses. Suitable precautions should be taken in the design of drive systems to minimize the magnitude of these spikes.

When operated under normal service conditions where the inverter input nominal voltage does not exceed rated motor voltage, stator winding insulation systems for definite purpose inverter fed motors shall be designed to operate under the following limits at the motor terminals.

Motors with base rating voltages V_{rated} 600 volts:

$$V_{peak} \leq 1.1 * 2 * \sqrt{2} * V_{rated} = 3.1 * V_{rated}$$

$$Rise\ time \geq 0.1\mu s$$

See Fig. 2.1 for a typical voltage response at the motor terminals for an illustration of V_{peak} and rise time. Motors with base rating voltage $V_{rated} > 600$ volts:

$$V_{peak} \leq 2.5 \left(\frac{\sqrt{2}}{\sqrt{3}} \right) V_{rated} = 2.04 * V_{rated}$$

$$Rise\ time \geq 1\mu s$$

Where: V_{peak} is a single amplitude zero to peak line to line voltage.

V_{rated} is the rated line to line voltage.

When the input voltage to the inverter exceeds the rated voltage, care must be taken in determining the maximum peak voltage V_{peak} that will be applied to the motor by the inverter.

2.3 International Electrotechnical Commission Standards IEC 60034-18-41

This standard defines criteria for assessing the insulation system of stator windings which are subjected to pulse width modulation drives. Also regarding to the qualification and type test I electrical insulation system used in rotating electrical machines fed from voltage converters. The necessary normative references and definitions are given together with a review of the effects arising from converter operation. Having established the technical foundation for the evaluation procedure, the conceptual approach is then described. This is to divide the systems into those which are not expected to experience partial discharge activity in their service lives (Type I) and those which are expected to withstand partial discharge activity throughout their service lives (Type II).

The Type I is generally used in rotating machines rated at less than 700 V and tend to have random wound stators. The procedures described here are directed at; qualification of the insulation system and type testing of the complete stators of service machines.

Before undertaking any testing, the manufacturer must decide upon the level of severity that the system will be required to withstand. The severity is based on how large the voltages overshoot and how short the impulse rise time will be at the machine terminals. It is important for the drive system integrator to characterize what the worst-case overshoot voltage and the shortest voltage rise time the winding will experience. The motor designer then makes choices from a table in which the complete ranges of expected values for these two independent parameters are divided into bands. Testing is performed at the extreme value of each band.

The impulse test equipment, are described in IEC 61934.

Modern converter output voltage rise times may be in the 50 ns to 2000 ns range due to power semiconductor switching characteristics. The voltage at the terminals of a converter driven machine depends several characteristics of the power drive system such as; operating line voltage of the converter, architecture and control regime of the converter, filters between the converter and motor, length of cable between them and design of the machine winding.

Voltages above $2 * V_{dc}$ can be produced at the terminals of the machine by drive double transition and by a converter fed drive algorithm that does not allow a minimum time between successive impulses. Double transition occurs, for example, when one phase

switches from minus to plus V_{dc} at the same time that another phase switches from plus to minus. This generates a $2 * V_{dc}$ voltage wave which travels to the machine and can then increase in magnitude when reflected at the machine terminals. If there is no minimum impulse control in the drive and if the time between two impulses is matched with the time constant of the cable between the drive and the motor, an over voltage of $2 * V_{dc}$ will occur at the machine terminals. The reflection can be reduced or prevented by using a filter in the converter or at the machine terminals.

If a winding experiences short rise time impulses with significant magnitude, high voltage stresses will be created in the insulation between conductors in different phases, between a conductor and ground, and between adjacent turns in the line and coil. Due to space and surface charge creation within the insulation components, the electric stress is not defined by the instantaneous voltage itself but also by the peak voltages that have been stressing the insulation previously. Generally, it has been shown by experience that, within certain limits valid for drive systems, the stressing parameter is the peak to peak voltage.

2.3.1 Partial Discharge and Insulation

In a low voltage, random or form wound winding, the conductor insulation has a small thickness, and there is often some air surrounding the wire. Additionally, in a random winding the first and last turns of one or more coils may be adjacent. With sufficient electric stress between turns, or to ground or to another phase, the air between the wires or to ground may experience electrical breakdown such as a spark in the air. Since the insulation itself does not break down, this spark is called partial discharge. The electrons and ions created by the discharge in air deteriorate the wire, ground or phase insulation. In random wound windings, conventional wire insulation is a thin organic film. This film is eventually eroded by the partial discharge, leading to insulation failure and a shorted coil. Pitting of the wire insulation and white powders are typical observable indications that partial discharge has occurred in service. The ground insulation of high voltage winding may be attacked by PD but the designer can allow the presence of partial discharges by incorporating materials that are resistant to deterioration by them. A further factor which may influence the life of the insulation is the effect upon dielectric heating of the higher frequencies associated with the converter waveform. Both the repetition frequency and the frequency associated with the rise

time of the leading edge will create extra heating through the dielectric losses in the insulation materials. The most critical regions are the main wall insulation in the stator slots.

2.3.2 Partial Discharge measurements

Conventional PD measurement devices for use with 50/60Hz voltages such as described in IEC 60270, cannot generally be used the applied voltage is a short rise time voltage impulse. A rise time of 100ns has a harmonic content with frequencies of more than 3 MHz; this means that the voltage impulse will have components within the pass band of most IEC 60270 style detectors, resulting in a displayed signal that may be hundreds of times the magnitude of the partial discharge pulses. For this reason, the partial discharge pulses will be difficult to distinguish from the high frequency components of the voltage impulses. In addition, the voltage impulses may be of sufficiently high magnitude to destroy the electronics of the partial discharge detector. To distinguish the partial discharge from the short rise time components of the voltage impulses, a different type of PD detector is needed. The detector should reduce all frequency components from the voltage to less than the high frequency components associated with the partial discharges. The display can be a standard oscilloscope or a pulse magnitude analyzer. Guidance is given in IEC 61934 on the method equipment to be used. The measurement of PD caused by short rise time impulses is an emerging technology and some skill may be required to separate PD from any residue of the impulse voltage. Without such skill, a test object may be classified as having a lower PDIV than it actually has. Conversely, PD remote from the PD sensor may not be detected. Thus, care must be taken with these PD measurements.

In general, the sensitivity of a partial discharge detector falls as the impedance of the load decreases (or its capacitance increases). As a guide, the sensitivity expected for qualification and the type test should be 1pC per nF of capacitive load at 50/60Hz, with a minimum sensitivity of 1pC. A measurement system capable of achieving this degree of sensitivity is considered to be sufficiently sensitive to make PDIV measurements on inductive loads when equating impedances. When PD is to be measured in test object energized by voltage impulses, the background noise should be measured in mV according to the procedure in IEC 61934. The repetitive PD inception voltage is determined according to IEC 61934. The background noise level is given in mV. This background noise level and the sensitivity according to IEC 61934 shall be reported.

2.4 International Electrotechnical Commission IEC Technical Specification 61934

2.4.1 Measurements of PD under short rise time and repetitive voltage impulses

In this standard are exposed configurations of electrical measurements of partial discharges that occur in electrical insulation system when stressed by repetitive voltage impulses having a rise time of $50\mu\text{s}$ or less.

IEC 60270 describes the methods employed to measure the electrical pulses associated with PD in test objects excited by DC and alternating voltages up to 400Hz. The methods used to measure PD pulses when the test object is subjected to supply voltage impulses should normally be modified from the standard narrow-band frequency methods described in IEC 60270.

To measure the PD during repetitive short rise time voltage impulses, the detector circuit shall be of the ultra-wide band where the operating detection range is such that exciting impulse voltage is strongly suppressed while the PD pulse is not significantly suppressed. IEC 60270 does not suggest specific ultra-wide band detection methods. For the purposes of IEC 61934 technical specification, specific detection methods are required.

The measured quantities concern the repetitive partial discharge inception voltage (RPDIV), the repetitive partial discharge extinction voltage (RPDEV) and partial discharge pulse repetition rate. PD readings are reported in units of mV, RPDIV and RPDEV may depend on PD measurement sensitivity and measurement circuit noise.

The test object behave predominantly as inductive, capacitive or distributed equivalent impedances according to the voltage supply frequency content. For some test objects, whether they are predominantly inductive, capacitive or distributed may depend on the PD detection frequency range (not only on the voltage supply frequency). Test objects with distributed behavior have transmission line which may cause attenuation and distortion of the PD pulses propagates through the test object.

2.4.2 Testing conditions

PD pulses can occur during the rise time of a voltage impulse or the remaining period of the impulse. PD depends on the testing conditions, including supply voltage impulse, environmental factors, as well as from ageing extent. For this reason, comparative evaluations should be carried out using test circuits and generators having the same characteristics, and comparable environmental conditions. Measurement of PD quantities at different times during the service life of a test object can be used as a diagnostic technique to assess the degree of ageing of the insulation system and form the basis of condition-based maintenance procedures.

The RPDIV, RPDEV and, in general, PD associated quantities will depend upon specific features of the waveform, for example the impulse rise time, the impulse decay time, the impulse repetition rate and the number of oscillations in the impulse. For the purpose of comparison between different can be performed using solutions, partial discharge measurements can be performed using standardized voltage supply waveform. The appropriate impulse waveform can depend on the type of test object and the type of application. The specification of the impulse supply should include, amongst other factors: impulse rise time, impulse voltage polarity, impulse voltage repetition rate, impulse width and impulse duty cycle.

The environmental factor on RPDIV and RPDEV, PD associated quantities may be affected by the following factors: humidity, temperature, degree of contamination of the test object, atmospheric pressure and type of gas.

2.4.3 PD detection methods

Any PD pulse detection system, where the test object is excited by voltage impulses, requires strong suppression of the residual voltage impulse, measured by the PD detection circuit, and negligible suppression of the PD pulse. The PD pulse shall have a magnitude after processing by the detection system that is greater than the residual transmitted voltage impulse. The amount of impulse voltage suppression required will be dependent on the test voltage and the rise time of the impulse. As the impulse voltage increases in amplitude, greater suppression is

required in order to ensure that important PD pulse magnitudes are higher than the residual transmitted voltage impulse on the output of the detector. Similarly, as the rise time of the applied impulse voltage becomes shorter, the suppression should be greater, due to the increased overlap of frequency spectra of supply impulse and PD pulse. PD pulse coupling devices shall be designed in order to ensure that important PD pulse magnitudes are higher than the residual transmitted voltage impulse on the output of the detector.

2.4.4 PD sensors

PD current or voltage pulses in a test object can be detected either by means of high voltage capacitors, high frequency current transformers (HFCT) or electromagnetic couplers such as antennas. The detectors, in conjunction with the rest of the measuring system, must be able to suppress the impulse voltage to a magnitude less than that expected from the PD pulse using appropriate filters.

The coupling capacitor should have a voltage rating exceeding the expected applied impulse voltage, together with a filter that strongly attenuates the test voltage impulses, can be used. The filter should have at least three poles and special measures to inhibit cross coupling of the input signal to the output. The filter can be designed using passive or active filtering technology. The coupling capacitor is connected to the test object high voltage terminal.

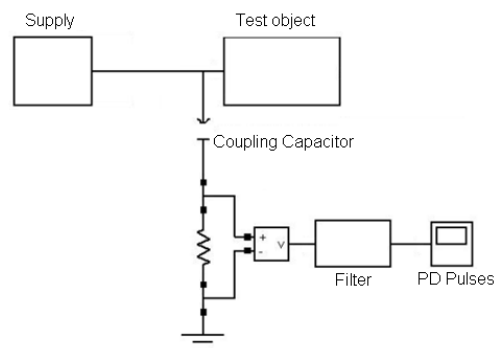


Fig. 2.4 PD Test with Coupling Capacitor and Multipole Filter

To display the PD signal output from the coupler and detection system can be recorded on a digital oscilloscope or pulse magnitude analyzer. For oscillographic display, the PD output is

normally displayed on one channel, while a reduced magnitude version of the applied impulse voltage is recorded on another channel. The magnitudes of the PD pulses as well as the temporal position in which they occur with respect to the impulse voltage are recorded. The RPDIV and RPDEV, as well as, in general, PD associated quantities, depend on the sensitivity of the measuring system to PD and how well the PD pulses can be distinguished from other electrical interference or noise such as the residual signal from the voltage impulse itself. Thus the sensitivity of the PD measuring system shall be assessed and recorded. The sensitivity is measured in mV.

The impulse supply should be as physically close to the test object as possible, in order to prevent attenuation and dispersion of the applied impulse due to the equivalent transmission parameters of the connecting leads. Earth loops should be avoided. The PD detector should be as close as possible to the test object, Since the PD is measured with a ultra-width band detection system, grounding of the test object should be made directly to the impulse voltage supply, with leads as short as possible and with low inductance.

Chapter III: Models

3.1 Description of Universal AC Rotating Machine Model

The construction of an accurate electric model for an induction motor has been widely developed for normal sinusoidal voltage feeding, and transient conditions. When the motor is fed through a power IGBT converter, the voltage is no more sinusoidal but made of rectangular pulses with rising rate in the order of $\text{kV}/\mu\text{s}$. With this wave shape feeding the motor, a lot of high order harmonic voltage components are introduced in the power line. The capacitive elements coupling the stator windings, the frame and the rotor are not irrelevant in this case since the voltage feeding the winding has a very high rise time. In a linking capacitor even of 1nF , stressed by a $1\text{kV}/\mu\text{s}$ rising rate voltage, flows a current of 1A . Other studies related these phenomena to the shaft voltage and relevant capacitive couplings in a motor structure, as presented in [26].

The new universal induction motor model [27]-[28] is built to predict the behaviour of the motor from low to high frequency. This new model is built using some LCR bridge measurements in differential mode (DM). Differential mode measurements are made with two motor phase terminals linked together as one connector to the LCR bridge and the other

phase terminal as the second connector as in Fig. 3.1. The motor is put on an insulating layer to obtain good data precision. In fact, if the motor frame was grounded, the test current may be drawn to ground and not read by the bridge.

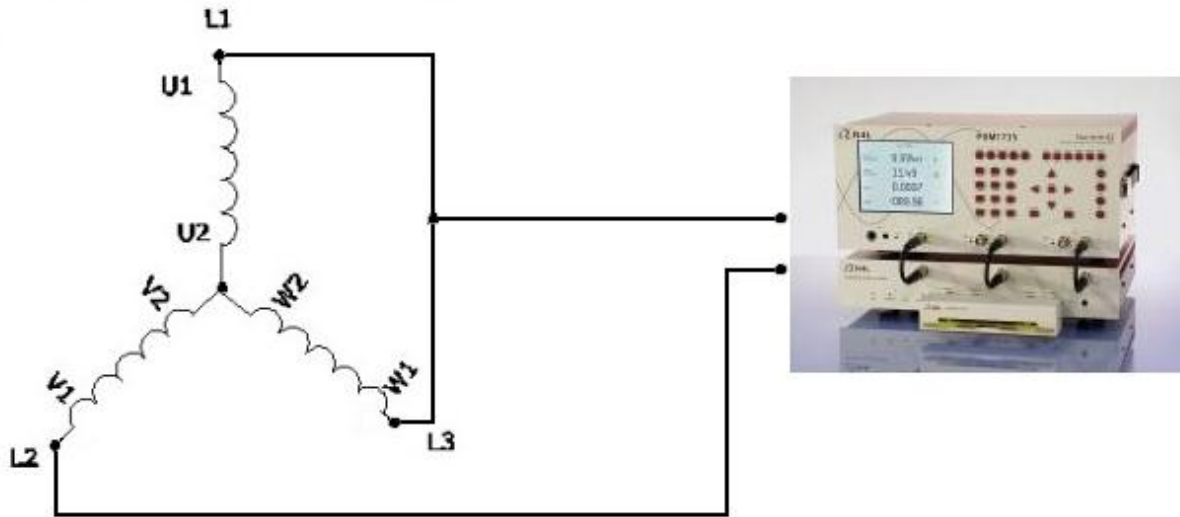


Fig. 3.1 LRC Bridge and AC Rotating Machine Differential Mode connection (DM)

With this configuration, it is possible to obtain the differential mode frequency response of the motor. The range of frequency must be wide enough to include the low, medium and high frequency response of the motor. A good range is 100Hz – 10MHz.

From the impedance and phase vs. frequency response, some particular values can be obtained.

Absolute impedance and the frequency at which the phase reaches its maximum value:

$$|Z(f(\varphi_{Max}))|, f(\varphi_{Max}) \quad (3.1)$$

Absolute impedance and frequency at the first resonance point. The impedance at the resonance point is in the maximum value:

$$|Z|_{MAX}, f_r \quad (3.2)$$

Absolute impedance and the frequency related at the first anti-resonance point (minimum point):

$$|Z(fa)|, fa \quad (3.3)$$

Absolute impedance and the frequency related at 10^{-3}Hz (1mHz) or DC measurement:

$$|Z(f_{DC})|, f_{DC} = 1\text{mHz}. \quad (3.4)$$

From LCR Bridge measurements between one phase of the motor in Y connection and the second probe connected to the frame, the following can be obtained:

Winding to frame capacity at high frequency

$$(f = 1\text{MHz}) \quad \text{This is } C_{sf-HF} \quad (3.5)$$

Winding to frame capacity at low frequency

$$(f = 1\text{kHz}) \quad \text{This is } C_{sf-LF} \quad (3.6)$$

The elements in the model that represent the classical model for low frequency are magnetizing inductance Lm , leakage inductance L_{1r} , iron loss resistance R_{core} , rotor equivalent load resistor R_r/s and DC-resistance R_s as shown in Fig. 5.6. The other elements represent the high frequency phenomena. The leakage inductance of the first turns of the winding ηL_{1S} , leakage inductance of the other turns L_{1S} , stator winding to stator frame capacity C_{sf} , high frequency resistance R_{sf} , equivalent capacity between the turns of the winding C_{sw} , total loss equivalent resistance R_{sw} . The neutral point is coupled to ground by the capacity C_{sf-0} .

Using the measured value of impedance and capacity as initial data (3.1) – (3.6) and the relations (3.7) – (3.17) as suggested and explained in [28], all the elements value can be obtained. From the manufacturer data, Lm and R_{core} are derived.

$$R_s = \frac{2}{3} |Z(f_{DC})| \text{ or from constructor data-sheet} \quad (3.7)$$

$$R_w = R_s \text{ (Slip } s=1) \quad (3.8)$$

$$L_{1s} = L_{1r} = \frac{\sqrt{\left[\frac{2}{3}Z(f(\varphi Max))\right]^2 - (2R_s)^2}}{4\pi \cdot f(\varphi Max)} \quad (3.9)$$

$$C_{sw,HF} = \frac{2\omega_r^2 L_{1s} C_{sf,HF} - 1}{\omega_r^2 L_{1s} (\omega_r^2 L_{1s} C_{sf,HF} - 1)} \text{ (Y connection)} \quad (3.10)$$

$$C_{sw,LF} = \frac{2\omega_r^2 L_{1s} C_{sf,LF} - 1}{\omega_r^2 L_{1s} (\omega_r^2 L_{1s} C_{sf,LF} - 1)} \text{ (Y connection)} \quad (3.11)$$

$$C_{sw} = \frac{C_{sw,HF} + C_{sw,LF}}{2} \quad (3.12)$$

$$C_{sf} = C_{sf,HF} \quad (3.13)$$

$$R_{sf} = \frac{2}{3} |Z(fa)| \quad (3.14)$$

$$\eta L_{1s} = \frac{1}{C_{sf-HF} * (2\pi fa)^2} \quad (3.15)$$

$$R_{sw} = \frac{2}{3} |Z|Max - |R_{core} // (j2\pi fr L_{1r})| \quad (3.16)$$

$$C_{sf-0} = C_{sf-LF} - 3C_{sf-HF} \quad (3.17)$$

3.2 Description of Cable Model

The model cable used in this thesis is based on Distributed parameters. Distributed parameters representation provides accurate results in the study of high frequency transients than the lumped-parameter models [29]-[30].

The paper on reference [31] proposes a three-phase transmission line model with the first successful use of Maxwell 2D Finite Element Analysis [32] to obtain the cable parameters RLC over a wide range of frequencies. Comparison between an expensive cable testing and predicted FEA are exposed in this section. The cable used for this exercise is a 3 conductor, 3 ground cable with copper tape shield as shown in Fig. 3.2.

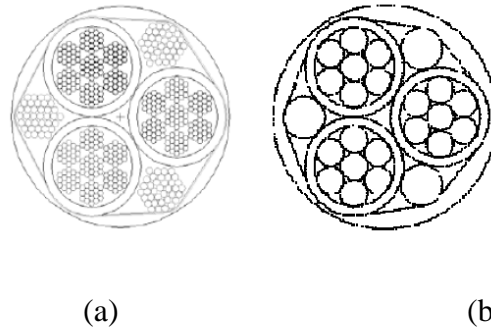


Fig.3.2 Detailed cross sectional geometry and Simplified for FEA simulation [31]

3.2.1 Impedance Measurement Technique for Cables

A 10 meter long cable is measured with a LCR meter, obtaining resistance, inductance and capacitance as a function of frequency in various DM and CM configurations. Figure 3.3 and 3.4 show the configuration of DM and CM switching states of a 6 switch inverter. The simulation models for reflected wave and CM analysis use parameters of the line-line three wire and line-ground three wire configuration respectively.

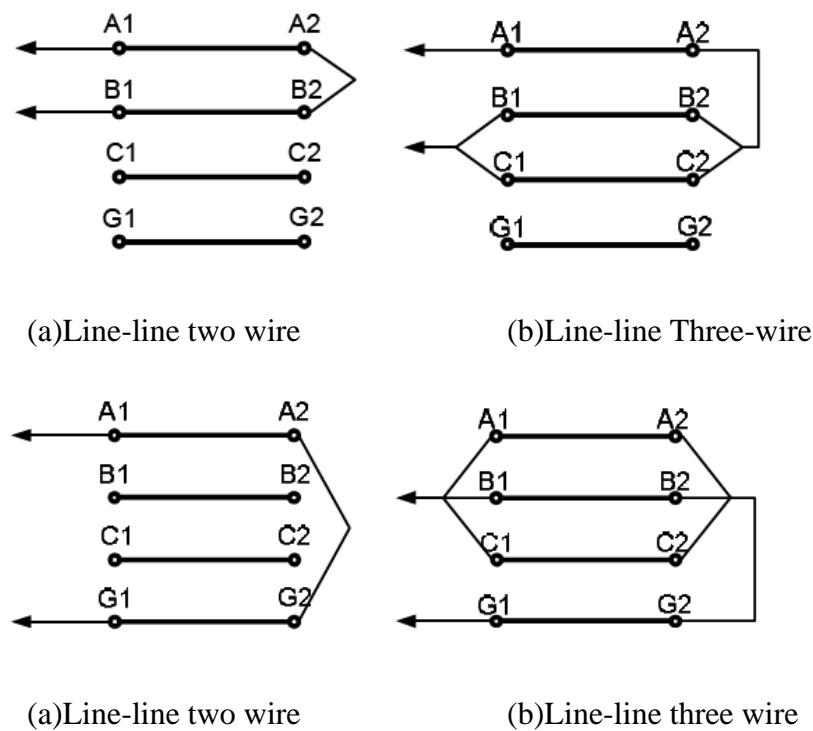
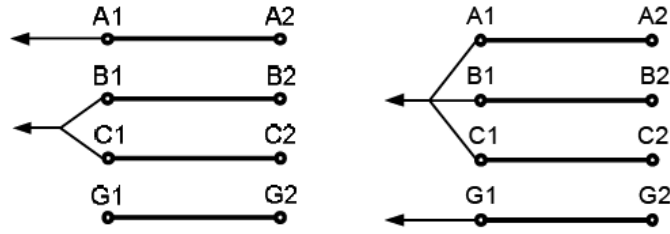


Fig. 3.3 CM cable configurations to determine inductance L_s and series resistance R_s



(a)DM Line-line three wire

(b)CM Line-ground three wire

Fig. 3.4 Measure of capacitance C_p and R_p

Now the resistance and inductances of any cable geometry are represented by 4x4 symmetrical matrix and the capacitances are represented by a 3x3 symmetric matrix, approach proposed by [31]. In matrix L, diagonal elements represent self-inductances and off diagonal elements represent mutual inductances. The R and L matrices vary with frequency while the capacitance matrix does not vary with frequency.

$$R = \begin{bmatrix} R_g & R_{ga} & R_{gb} & R_{gc} \\ R_{ga} & R_a & R_{ab} & R_{ac} \\ R_{gb} & R_{ab} & R_b & R_{bc} \\ R_{gc} & R_{ac} & R_{bc} & R_c \end{bmatrix} \quad (3.18)$$

$$L = \begin{bmatrix} L_g & M_{ga} & M_{gb} & M_{gc} \\ M_{ga} & L_a & M_{ab} & M_{ac} \\ M_{gb} & M_{ab} & L_b & M_{bc} \\ M_{gc} & M_{ac} & M_{bc} & L_c \end{bmatrix} \quad (3.19)$$

$$C = \begin{bmatrix} C_{ag} & C_{ab} & C_{ac} \\ C_{ab} & C_{bg} & C_{bc} \\ C_{ac} & C_{bc} & C_{cg} \end{bmatrix} \quad (3.20)$$

Measured inductance and capacitance for configurations shown on Fig. 3.3 and 3.4 are related to the L matrix, assuming cable geometry symmetry between the three phases:

$$\text{Line - line three wire } L = \frac{3}{2}(L_a - M_{ab}), C = 2C_{ab} + \frac{2}{3}C_{ag} \quad (3.21)$$

$$\text{Line - ground three wire } L = \frac{1}{2}(L_a - 2M_{ab}) + (L_g - 2M_{ag}), C = 3C_{ag} \quad (3.22)$$

3.2.2 Finite Element Analysis Simulation

The Finite Element Analysis (FEA) is a numerical technique for finding approximate solutions of partial differential equations and integral equations; based on eliminating the differential equation becoming on steady state. Also the partial differential equation is rendering into ordinary differential equation, and finally integrated using standards methods such as Euler.

The finite element software used is reported on reference [32] with setting on electrostatic field solver to determine the capacitance matrix and eddy current solver to determine inductance and series resistance matrices as a function of frequency. In this solution the skin effect are included. Figure 3.2 (b) represents the simplified model in order to reduce the time simulation without significant accuracy compromising. While Fig. 3.2 (a) represents the real geometry of cable.

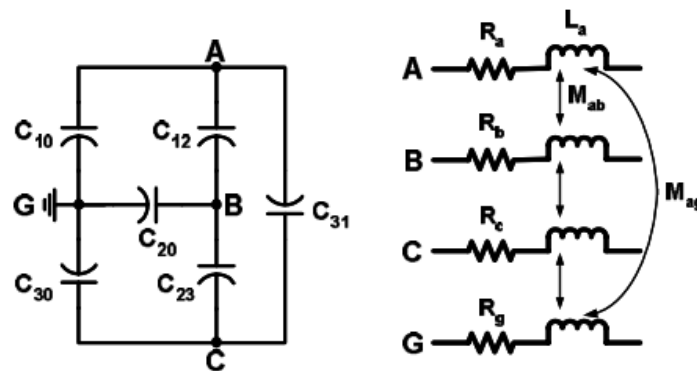


Fig.3.5 Circuitual representation of parameters to be able to extract from FEA simulation [31]

The range of frequency from samples on simulation is from 100Hz to 1MHz and the matrix are similar compared with the ones from measurements. Matrix on FEA the off diagonal elements in R matrix are small and can be neglected for simulation.

The changes on capacitances are without significance with the variation of frequency on FEA electrostatic field solver and measurements on laboratory. On the simulation the matrix C has an interpolation based on solving for electrostatic charge Q using the equation $Q = CV$ and the sum of all values of Q is equal to zero [31]. The equation (3.23) is represented by 3 linear equations expressing charge Q as a function of voltage.

$$\begin{aligned}
Q1 &= c_{11}V_1 + c_{12}V_2 + c_{13}V_3 \\
Q2 &= c_{21}V_1 + c_{22}V_2 + c_{23}V_3 \\
Q3 &= c_{31}V_1 + c_{32}V_2 + c_{33}V_3
\end{aligned} \tag{3.23}$$

According to the electrostatic solver the c_{ii} are capacitive coefficients and the diagonal c_{ij} are inductive coefficients, which has inverse values between them. Coefficients of capacitance are positive and coefficients of inductance are negative, because Q_i is positive, then V_i is positive, thus the Q_j induced results to be negative. According to scheme on Fig. 3.5 the equation will be,

$$\begin{aligned}
Q1 &= c_{10}V_1 + c_{12}(V_1 - V_2) + c_{13}(V_1 - V_3) \\
Q2 &= c_{12}(V_2 - V_1) + c_{20}V_2 + c_{23}(V_2 - V_3) \\
Q3 &= c_{13}(V_3 - V_1)V_1 + c_{23}(V_3 - V_2)V_2 + c_{30}V_3
\end{aligned} \tag{3.24}$$

The conductor to ground capacitances c_{10} , c_{20} and c_{30} are the self-partial capacitances. The line-line capacitances c_{ij} are the mutual partial capacitances. Equation (3.25) is the arrangement of (3.24) in Y coefficient matrix.

$$\begin{aligned}
Q1 &= (c_{10} + c_{12} + c_{13})V_1 - c_{12}V_2 - c_{13}V_3 \\
Q2 &= -c_{12}V_1 + (c_{20} + c_{12} + c_{23})V_2 - c_{23}V_3 \\
Q3 &= -c_{13}V_1 - c_{23}V_2 + (c_{30} + c_{13} + c_{23})V_3
\end{aligned} \tag{3.25}$$

The coefficient in (3.23) is related to the capacitance shown in Fig. 3.5. Equation (3.26) becomes from (3.23) and (3.25).

$$\begin{aligned}
c_{11} &= c_{10} + c_{12} + c_{13} & c_{12} &= -c_{12} \\
c_{22} &= c_{12} + c_{20} + c_{23} & c_{23} &= -c_{23} \\
c_{33} &= c_{13} + c_{23} + c_{30} & c_{13} &= -c_{13}
\end{aligned} \tag{3.26}$$

The coefficient of capacitance c_{ii} is equal to the total capacitance between conductor i and ground, with all other conductors shorted to ground in Fig. 3.5. The c_{ij} coefficients of induction have inverse value of the mutual partial capacitances c_{ij} . The simulation programs require a physical realizable matrix of the form in (3.18) using c_{10} , c_{20} , and c_{30} conductor-to-

ground self-partial capacitances and c_{ij} line-line mutual partial capacitances. The c_{ij} terms can be determined from above. Line-to-ground self-partial capacitances are shown in (3.27)

$$c_{11} = c_{10} + c_{12} + c_{13}$$

$$c_{22} = c_{12} + c_{20} + c_{23}$$

$$c_{33} = c_{13} + c_{23} + c_{30}$$

$$C = \begin{bmatrix} Cag & Cab & Cac \\ Cab & Cbg & Cbc \\ Cac & Cbc & Ccg \end{bmatrix} = \begin{bmatrix} C10 & C12 & C13 \\ C12 & C20 & C23 \\ C13 & C23 & C30 \end{bmatrix} \quad (3.27)$$

The distributed parameter multiphase model of Matlab Simulink [33] SimPowerSystems should be converted from matrix parameters to positive (3.28) and zero (3.29) sequence in order to put the values on the block parameters.

$$C1 = Cag - Cab = pF/m \quad (3.28)$$

$$C0 = Cag + 2Cab = pF/m \quad (3.29)$$

And for inductances positive sequence is according to equation (3.30) and zero sequence on equation (3.31)

$$L1 = La - Mab = \mu H/m \quad (3.30)$$

$$L0 = La + 2Mab + 3(Lsg - 2Mag) = \mu H/m \quad (3.31)$$

In order to obtain the AC resistance, the DC resistance values must be multiplied by the skin effect factor of the cable [31].

3.2.3 Comparison between Measurements and Finite Element Results

A cable were measured using LCR meter, in a frequency range from 20Hz to 1Mhz and also modeled in FEA software to obtain the RLC matrices.

Between FEA and measurements, Inductance and resistance differences can be attributed to several factors including limitations of 2-D modeling cannot account for 3-D effects such as twisting of conductors. The accuracy of FEA simulation is typically about 5%. The accuracy

of LCR meter measurement and the fact that solid grouped conductor approximations were used instead of the multi-strand wires. Differences between LCR measurements and FEA inductance/resistance simulations are about 5 – 10 %.

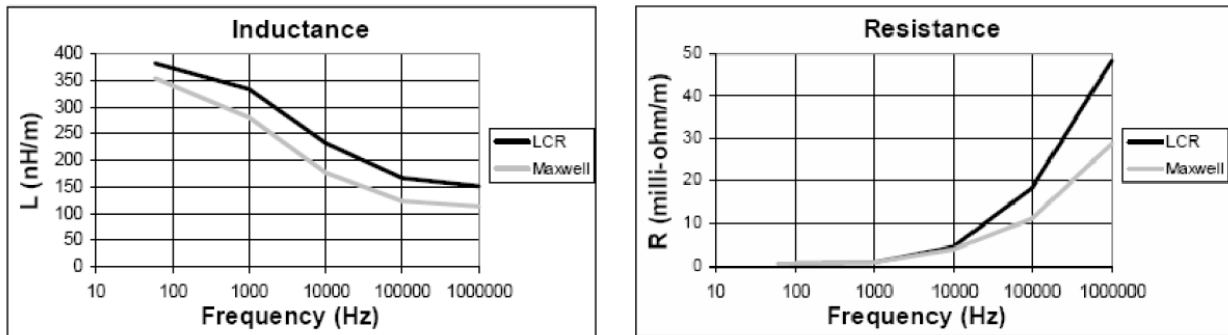


Fig. 3.2 Comparison Inductance and resistance for line-line three wire DM [31]

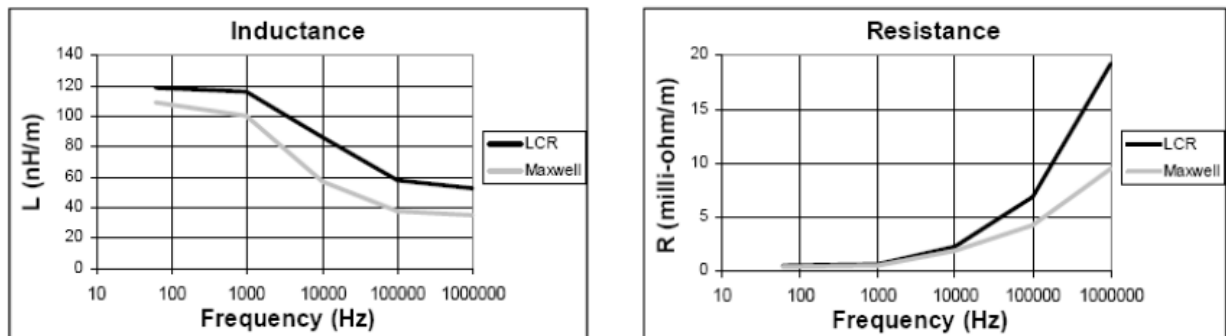


Fig. 3.3 Comparison Inductance and resistance for line-line three wire CM [31]

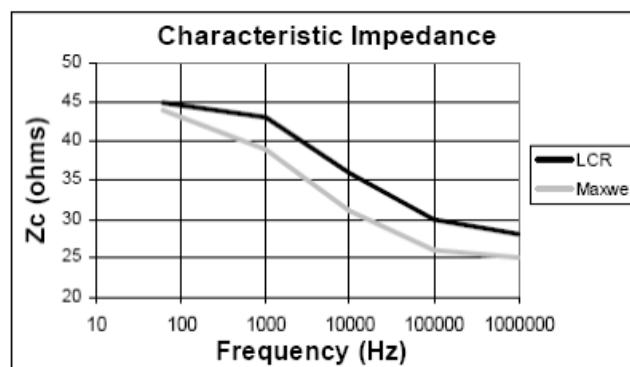


Fig.3.4 Characteristic Impedance

The 3-wire common mode capacitance of cable predicted by FEA was within 5% of measured LCR values. The 3-wire DM capacitance of the focus cable FEA prediction was within 20 % of the measured LCR value. Differences can be attributed to several factors including value of dielectric constant of conductor insulation, accuracy of FE simulation (typically about 5%) and LCR meter measurement accuracy. The capacitance of the cable does not vary with frequency variations [31].

Chapter IV: Filters

Efficiency and productivity improvements through variable frequency drives (VFD) have been increased on low and medium voltage ac induction motors. The machines are operated with pulse width modulation voltage (PWM) source inverters from 0.1 to 800 kW using insulated gate bipolar transistors (IGBT) as the preferred semiconductor switching device. IGBT switching time of 50 to 400ns is an order of magnitude faster than bipolar junction transistors (BJT), so IGBT drive switching efficiency is increased, drive package heat sinks are reduced, and higher carrier frequencies are possible. Also significant improves such as current waveform quality and reduction of audible noise in motor laminations. Cable application lengths for GTO and BJT switches allowed using longer cables before exceeding motor overvoltage dielectric capability. Moreover IGBT drives may create over-voltages that exceed the safe motor level with shorter cable lengths.

There are some conditions of PWM modulation cycle that, combined with long cable lengths, can lead to motor stress greater than the theoretical $2 * V_{dc}$ overvoltage with magnitudes of $3 * V_{dc}$ to $4 * V_{dc}$. When the transient has not fully decayed before the application of the next pulse, so that a residual trapped cable charge condition exists that may lead to $3 * V_{dc}$ overvoltage. The effects of these transients over $2 * V_{dc}$ are reported in [34] and shown to have adverse effects on motor dielectric life.

The overvoltage at the motor terminal can be analyzed with the voltage reflection theory for the cable end, which explains that the voltage overshoot depends on the inverter output voltage rise time, cable length, and the reflection coefficient of the cable end [35]-[36]-[37].

In this chapter different filter solutions are analyzed, in order to minimize the over voltage at the terminals of the motor.

4.1 Description of First Order RC Filter at Motor Terminals

In this solution the cable is terminated by a first order filter consisting of a capacitor in series with the resistor to match with the cable and provide the proper level of damping to control the voltage overshoot. The motor terminal overvoltage can be significantly reduced if at the cable end the impedance is equal to the cable surge impedance. Then the incident voltage will not be reflected and significant over-voltages at the terminals of the motor can be prevented. The derivations for the reflected wave equation due to an RC filter termination are illustrated. This solution is reported on [38]-[39].

The current and voltage in the incident wave is:

$$e_1 = Z_0 * i_1 \quad (4.1)$$

The currents and voltage of reflected wave are represented by equation (4.2) where the cable surge impedance is $-Z_0$.

$$e_2 = -Z_0 * i_2 \quad (4.2)$$

If

$$e_r = e_1 + e_2 \quad (4.3)$$

$$i_r = i_1 + i_2 \quad (4.4)$$

Where, e_r = voltage at the filter.

i_r = current through the filter.

When the serial RC filter is connected to the machine terminals, the boundary condition is:

$$e_r = R i_r + \frac{1}{c} \int i_r dt \quad (4.5)$$

Substituting equations (4.1) and (4.2) into equation (4.5) gives equation (4.6), which is the receiving end of the line.

$$e_1 + e_2 = R \left(\frac{e_1}{z_0} - \frac{e_2}{z_0} \right) + \frac{1}{c} \int \left(\frac{e_1}{z_0} - \frac{e_2}{z_0} \right) dt \quad (4.6)$$

$$(Z_0 + R) \frac{de_2}{dt} + \frac{e_2}{c} = (R - Z_0) \frac{de_1}{dt} + \frac{e_1}{c} \quad (4.7)$$

The shape of the first incident voltage is known and it is assumed to be $e_1 = E$, a flat topped constant voltage when the inverter switch is turned on. In this case the solution will be:

$$e_2 = E - K e^{-\frac{t}{(z_0+R)c}} \quad (4.8)$$

In order to determine the constant K, a boundary condition at the terminating end is required. The voltage across the capacitor cannot change instantaneously such that at time $t = 0$, the capacitor voltage is still zero or in other words, at this instant the capacitor is short-circuited. The incident voltage sees only a resistive component being applied at the terminal, and then the reflected voltage e_2 at $t = 0$ is:

$$e_2 = e_1 \frac{R-Z_0}{R+Z_0} \quad (4.9)$$

The equation (4.9) is placed into equation (4.8), and when time is zero K will be solve as shown is equation (4.10)

$$K = E \frac{2*Z_0}{(R+Z_0)} \quad (4.10)$$

The equation for the reflected voltage e_2 is:

$$e_2 = E - E \frac{2*Z_0}{(R+Z_0)} * e^{\frac{t}{(z_0+R)C}} \quad (4.11)$$

The voltage at the terminals of machine and filter will be:

$$e_2 = e_1 + e_2 = 2E - E \frac{2*Z_0}{(R+Z_0)} * e^{\frac{t}{(z_0+R)C}} \quad (4.12)$$

4.1.1 Design of RC Filter

To determine the values of R and C for the motor terminal filter, the first reflected wave have to be set equal to zero. That could be accomplished if $R = Z_0$ at the equation (4.9).

The value of capacitance has to fulfill the condition of limit the reflected wave from inverter, which should be $e_2 \leq 0.2 * E$ when it has been traveled twice trough the cable. The time which takes the wave to travel from inverter to the end of cable is:

$$t_t = \frac{l_c}{v} \quad (4.13)$$

$$v = \frac{1}{\sqrt{L_c * C_c}} \quad (4.14)$$

Where: l_c =cable length

L_c =Inductance per unit of length

C_c =Capacitance per unit of length

t_t =Time of pulse to transit from inverter to the machine

v =Pulse velocity

Then substituting in equation (4.11) leads to:

$$e_2 = E - E \frac{2*Z_0}{(Z_0+Z_0)} * e^{\frac{2*t}{(Z_0+Z_0)C}} = 0.2 * E \quad (4.15)$$

This equation is equal to,

$$E e^{\frac{2*t_t}{(Z_0+Z_0)C}} = 0.8 * E \quad (4.16)$$

$$C = -\frac{2(l_c\sqrt{L_c C_c})}{2Z_0 \ln(0.8)} \quad (4.17)$$

The surge impedance of cable is given by:

$$Z_0 = \sqrt{\frac{L_c}{C_c}} \quad (4.18)$$

And using (4.18) in (4.17) the capacitance will be:

$$C = \frac{l_c C_c}{0.22314} \quad (4.19)$$

4.2 Description of Second Order RLC Filter at Inverter Terminals

This solution consists on a RLC filter placed at the inverter terminals. It increases the rise time of the PWM output voltage applied to the cable, above a critical value reducing over-voltages due to reflections. Thus a low pass filter, as shown in Fig. 4.1, placed at the output terminals of the inverter can be specially designed to decrease the inverter output pulse dv/dt and thereby reduce the over-voltage and ringing at the motor terminals [40]-[41]-[42].

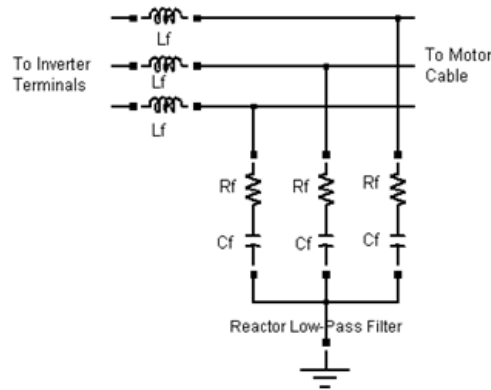


Fig. 4.1 LRC Filter

In equation (4.19) the critical rise time can be calculated for a give length of cable.

$$t_r = \frac{3 \cdot l_c \cdot \Gamma_L}{v \cdot 0.2} \quad (4.20)$$

Where: Γ_L =reflection coefficient at the load (typically 0.9 for motor less than 20hp)

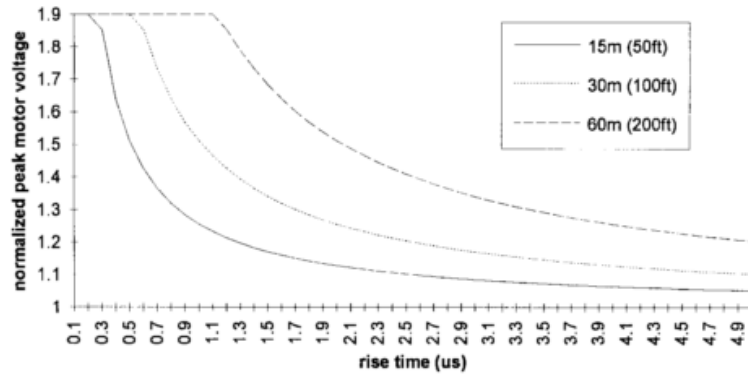


Fig. 4.2 Motor overvoltage vs. rise time for different cable length [43]

Increasing the rise time of the PWM inverter output, connected to a critical long cable, will reduce the over-voltages on machine terminals due to the reflections; this is verified by Fig. 4.2 from reference [43].

4.2.1 Design of LRC Filter

The series capacitor and resistor combination of this filter reduces the Joule effects of power losses across the damping resistor. The second order filter is found to yield the necessary stop band attenuation characteristics and the maximum ripple values in the pass band. Also the second order filter meets the conditions of limited number of components, reduced filter size, cost, and weight. The pass band represented by Butterworth filter is the appropriate thus the selected attenuation $A=3\text{dB}$. Then the value of H function that represents the behavior of the system is:

$$A = 20 \text{ Log } \left| \frac{1}{H} \right| \quad (4.21)$$

$$H = \frac{1}{10^{A/20}} \quad (4.22)$$

With equation (4.22) the value of H is found to be 0.707 and the cutoff frequency is represented by equation below.

The filter capacitor C_f represents a short circuit at high frequencies, R_f is set equal to the characteristic impedance of the cable Z_0 to absorb the reflected energy.

$$R_f = Z_0 = \sqrt{\frac{L_c}{C_c}} \quad (4.23)$$

$$R_f \geq \sqrt{\frac{4L_f}{C_f}} \quad (4.24)$$

To determine the cutoff frequency f_c , the critical rise time has to be known for a maximum of 20% of overvoltage. From Fourier series, the highest frequency component will determine the sharpness of a near square wave pulse; thus the cutoff frequency is:

$$f_c = \frac{1}{2 * t_{cr}} \quad (4.25)$$

And the angular velocity of the system will be:

$$\omega = 2\pi f_c \quad (4.26)$$

The Transfer function that represents the filter is:

$$H = \frac{1 + j\omega R_f C_f}{1 - \omega^2 L_f C_f + j\omega R_f C_f} \quad (4.27)$$

Considering vector form, through Pythagorean theorem turns to be

$$H^2 = \frac{(1)^2 + (\omega R_f C_f)^2}{(1 - \omega^2 L_f C_f)^2 + (\omega R_f C_f)^2} \quad (4.28)$$

Solving equation (4.24) by variable L_f

$$L_f = \frac{C_f R_f^2}{4} \quad (4.29)$$

Substituting (4.29) into (4.30)

$$H^2 = \frac{1^2 + (\omega R_f C_f)^2}{(1 - \omega^2 * ((R_f^2 * C_f) / 4) * C_f)^2 + (\omega R_f C_f)^2} \quad (4.30)$$

Solving by the variable C_f the equation (4.31) is found for value of every capacitor and from equation (4.29) the inductance values for the filter.

$$C_f = \sqrt{\frac{8 * (\sqrt{\frac{1 - (3 * H^2)}{4}}) - (4 * H^2) + 8}{(R_f * \omega * H)^2}} \quad (4.31)$$

Chapter V: Case Study 1. Reduction of Motor Overvoltage fed by PWM AC Drives using a Universal Model

An induction motor model construction and the validation of the model response to a filtering technique is analyzed in this chapter. The filter is connected to the rotating machine terminals in order to suppress over-voltages due to the long cables and high frequency pulses of the inverter. With the help of high frequency measurements made by the authors on a 1.1kW induction motor, an accurate simulation with Matlab SimulinkTM based on differential mode analysis, is made. The simulation shows realistic results for the determination of the filter parameters among different values of rise time and cable length.

5.1 Introduction

When ac rotating machines are fed by inverters based on insulated gate bipolar transistor (IGBT) technology, high frequency switching pulses feed the machine. With long cables, these pulses produce over-voltages at the motor terminals, causing a heavy electrical stress in the whole insulation system of the rotating machine. If this electrical stress is long-lasting and of a suitable high value, it drastically increases the aging of the insulation, with the consequence of partial discharge and destructive effects on windings, taking out of service the rotating machine and increasing the cost of the operations [44].

In the configuration shown in Fig. 5.1, the component models have been chosen in order to realize an effective simulation environment. The inverter model for the simulation allows the control of the rise time, in order to see the response of the components such as filter and machine. The high frequency parameters of the three phase cable model are calculated from LCR meter measurement [31].

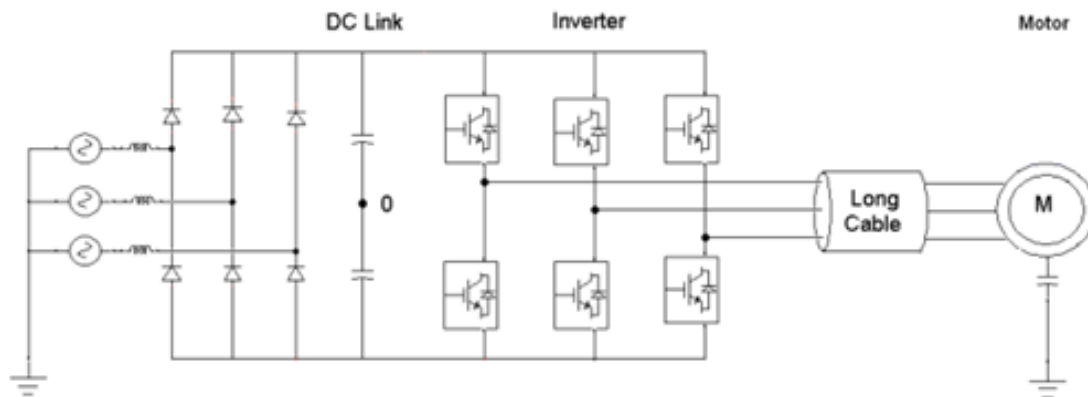


Fig. 5.1 Complete system for the analysis of overvoltage phenomenon

From the analysis at high frequency on the cable, it is possible to define the parameters of the filter: in this case an RC first order filter is used to reduce reflected wave at the motor terminals. This is a Line Termination Network (LTN) RC filter designed to match the surge impedance between the rotating machine and the cable as shown in Fig. 5.2. A design methodology to establish, in different situations, the optimum value of resistance and capacitance is presented in [39]-[43]-[45]. The length of cable and rise time will be variable for different simulations, to deeply observe the over-voltages and transients with or without the Line Termination Network RC filter.

The model of the rotating machine is universal in a way that it is constructed analyzing a wide range of low and high frequency effects, considering differential and common mode electric parameters, including high frequency leakage currents due to the effect of electromagnetic interference.

The authors of the motor model made analysis on the impedance frequency response in a wide range of frequency, obtaining the motor model parameters from few peculiar values [27]-[28]. In this chapter a 1.1kW four poles AC induction motor is analyzed to perform measurements of impedance and phase and build the model for the simulation. In this way we are able to compare the experimental results with the simulations.

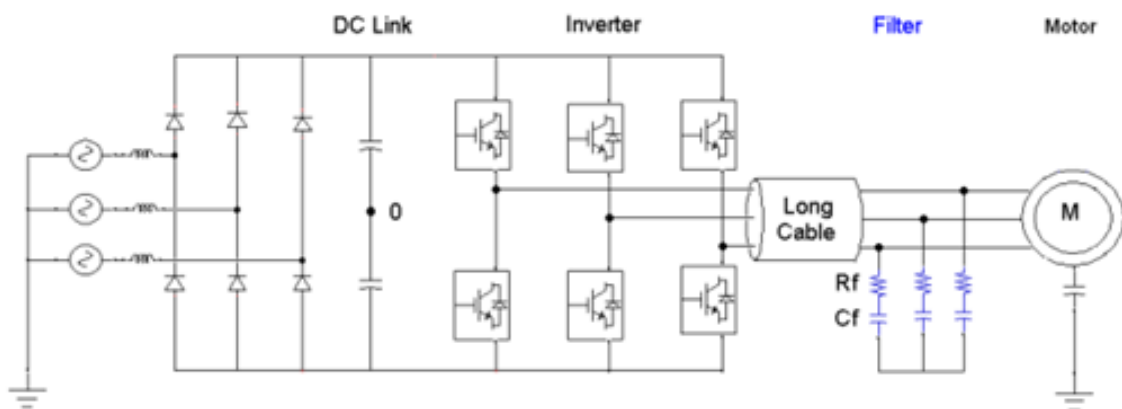


Fig. 5.2 System with LTN RC first order filter

5.2 Analysis of Components

In this section the design considerations for the components involved in the whole configuration shown in Fig. 5.2 are presented.

5.2.1 Three Phase Cable for PWM AC Drives

For the cable model the distributed parameters three phase line of SimPowerSystems™ has been used for the simulation. This model implements a 3-phase distributed LC parameter line with lumped losses. According to [31] the model has a good high frequency response. This is very important for investigating the high frequency phenomena due to the inverter feeding of

the motor. In order to obtain the R, L and C matrix for the model computation, the method suggested by [31] was resorted to. Measurements on an 11 AWG 4-conductors-PVC, 7.7m long cable, lead to the following matrices.

$$R = \begin{bmatrix} 17.8 & 0 & 0 \\ 0 & 17.8 & 0 \\ 0 & 0 & 17.8 \end{bmatrix} [m\Omega/m] \quad (5.1)$$

$$L = \begin{bmatrix} 909 & 552 & 552 \\ 552 & 909 & 552 \\ 552 & 552 & 909 \end{bmatrix} [nH/m] \quad (5.2)$$

$$C = \begin{bmatrix} 94.3 & -10.4 & -10.4 \\ -10.4 & 94.3 & -10.4 \\ -10.4 & -10.4 & 94.3 \end{bmatrix} [pF/m] \quad (5.3)$$

5.2.2 Application of First Order RC Filter at Motor Terminals

The RC filter is connected to the motor terminals in a Y connection as shown in Fig. 5.2. According to the approach proposed by [45]-[43]-[39], the filter resistance has to match the surge impedance of the cable.

$$R_f = Z_1 \quad (5.4)$$

Where the surge impedance of the cable is defined, at high frequency, by:

$$Z_1 = \sqrt{\frac{L_1}{C_1}} = \sqrt{\frac{(909-552)nH}{(94.3+10.4)pF}} = 58\Omega \quad (5.5)$$

As the motor surge impedance Z_m is greater than Z_1 [43]-[25], a parallel connected RC filter balances the motor impedance so that the equivalent total impedance Z_x is equal to the cable one Z_1 [39]-[43]. When the cable surge impedance Z_1 is equal to Z_x , the reflection coefficient in (5.6) is zero.

$$\Gamma = \frac{Z_x - Z_1}{Z_x + Z_1} = 0 \quad (5.6)$$

As a consequence, the reflecting wave is suppressed. To determine the value of the filter capacitance it should be known the rise time of the inverter pulse. At the very first time, the

filter acts like a pure resistor because the capacitor is uncharged. After the rise time, the capacitor is fully charged, acting like an open circuit and avoiding power dissipation. In [39] a simple RC charge equation is proposed considering a capacitor voltage value (V_{cx}) equal to 10% of the dc voltage (V_{bus}). It leads to the following equation:

$$V_{cx} = (0.10)V_{bus} = V_{bus}(1 - e^{-t_{rise}/(R_f C_f)}) \quad (5.7)$$

And from (5.7)

$$C_f = \frac{T_{rise}}{0.1054 * R_f} \quad (5.8)$$

With a typical inverter voltage rise time of 100ns, the capacitance turns out to be 16 nF.

5.3 Measurements Results

In the development of this thesis measurements were made, according to DM connection to a 1.1kW 50Hz, 380V four poles induction motor in a Y connection as shown in Fig. 5.3, with a Newtons4th Ltd PSM1735 Frequency response Analyzer [46]. From this measurement, the data is derived and reported in (3.1) – (3.6) in order to use the relations (3.7) – (3.17) to obtain the parameters shown in Table 5.2.



Fig. 5.3 Measurement with LRC Bridge on 1.1 kW AC induction motor

In Fig. 5.4, the display of the instrument shows the expected curve of impedance versus frequency, where it can be very clear the first anti-resonance point at 11.9MHz.

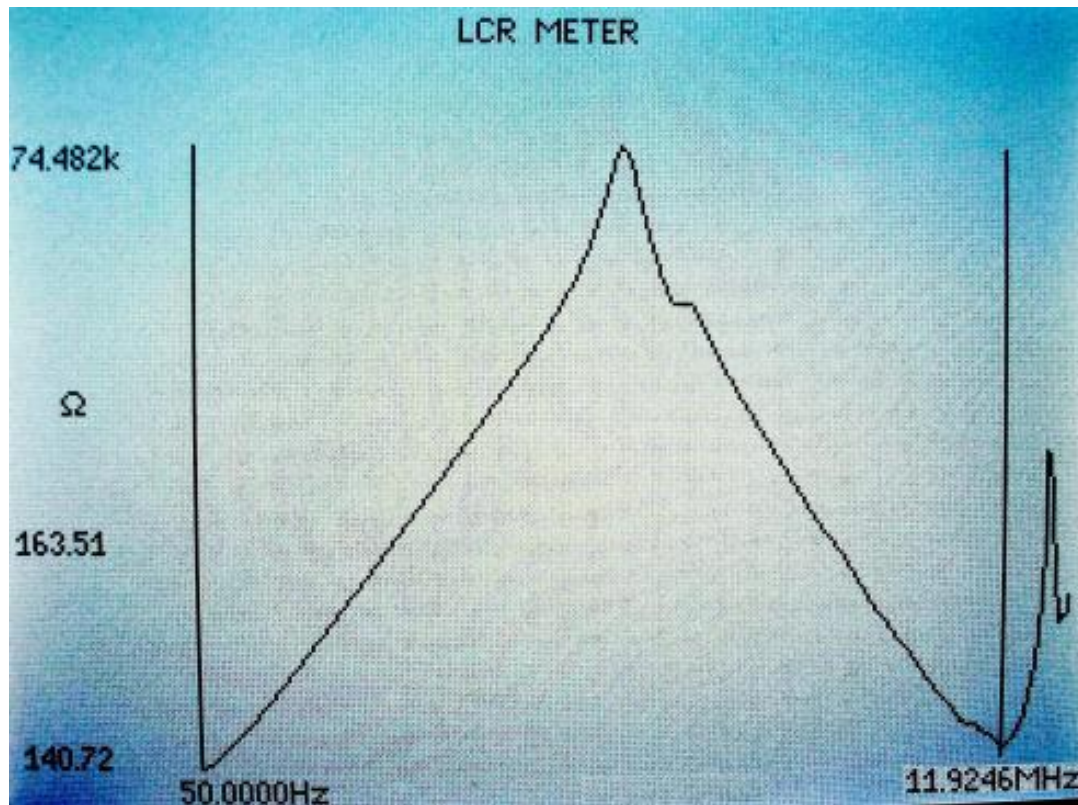


Fig. 5.4 Display of LRC Bridge for a frequency sweep on 1.1 kW AC induction motor

The data are reported in three frequency, impedance and phase, vectors. The same curve of impedance versus frequency and the phase versus frequency one, are then plotted in a Matlab™ file for analysis as shows in Fig. 5.5.

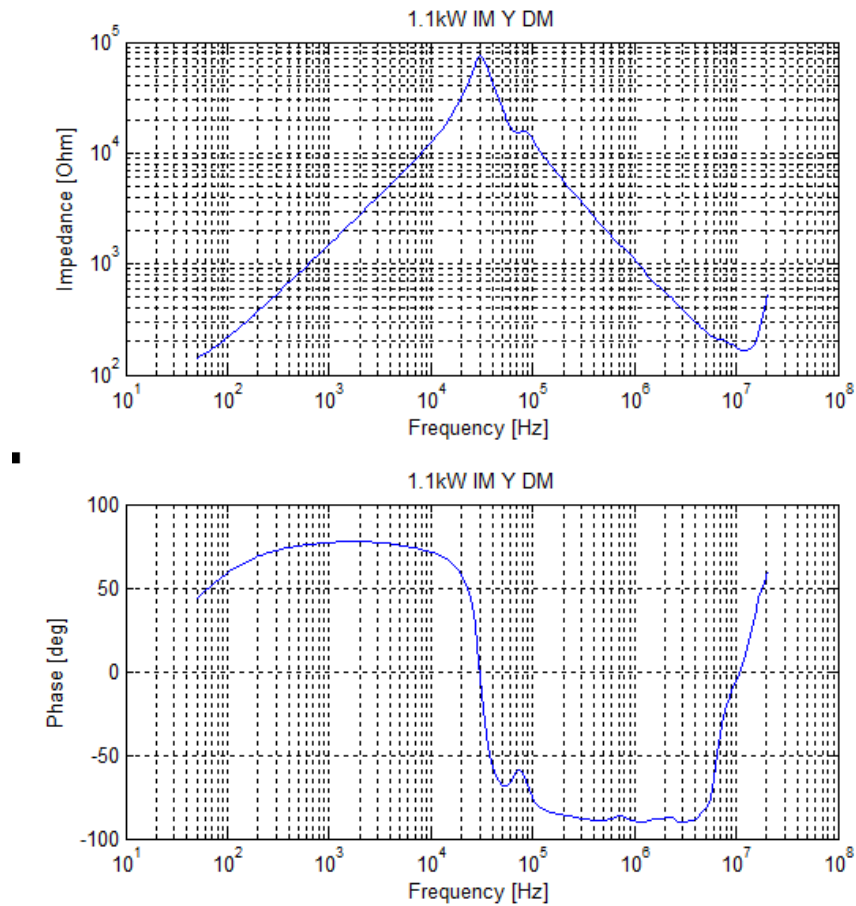


Fig. 5.5 Plot from measurement data 1.1 kW motor

5.4 Determination of Motor Parameters

The value of R_{core} and L_m can be obtained from the machine constructor, and those from the 1.1kW motor analysed on this thesis are shown on Table 5.1.

TABLE 5.1
PARAMETERS FROM THE MANUFACTURER DATA

Parameter	Value
L_m (mH)	350
R_{core} (Ω)	2500

Using measurement values for the 1.1kW machine in the equations (3.7) – (3.17) the values are reported in Table 5.2.

TABLE 5.2
PARAMETERS OF THE MOTOR MODEL

Parameter	Value
$R_r = R_s(\Omega)$	7.6
$L_{1s} = L_{1r}(mH)$	75.09
$C_{sw}(pF)$	494.2
$C_{sf}(pF)$	176.3
$R_{sf}(\Omega)$	109
$\eta L_{1s}(\mu H)$	1.01
$R_{sw}(k\Omega)$	47.19
$C_{sf-0}(pF)$	259.9

5.5 Simulations Results

In this chapter is built the Matlab Simulink™ model of Fig. 5.7, that includes the PWM inverter with adjustable rise time voltage front, the distributed line cable model based on data reported in Section 5.2.1, the three-phase induction motor model proposed of Fig. 5.6, and the RC filter.

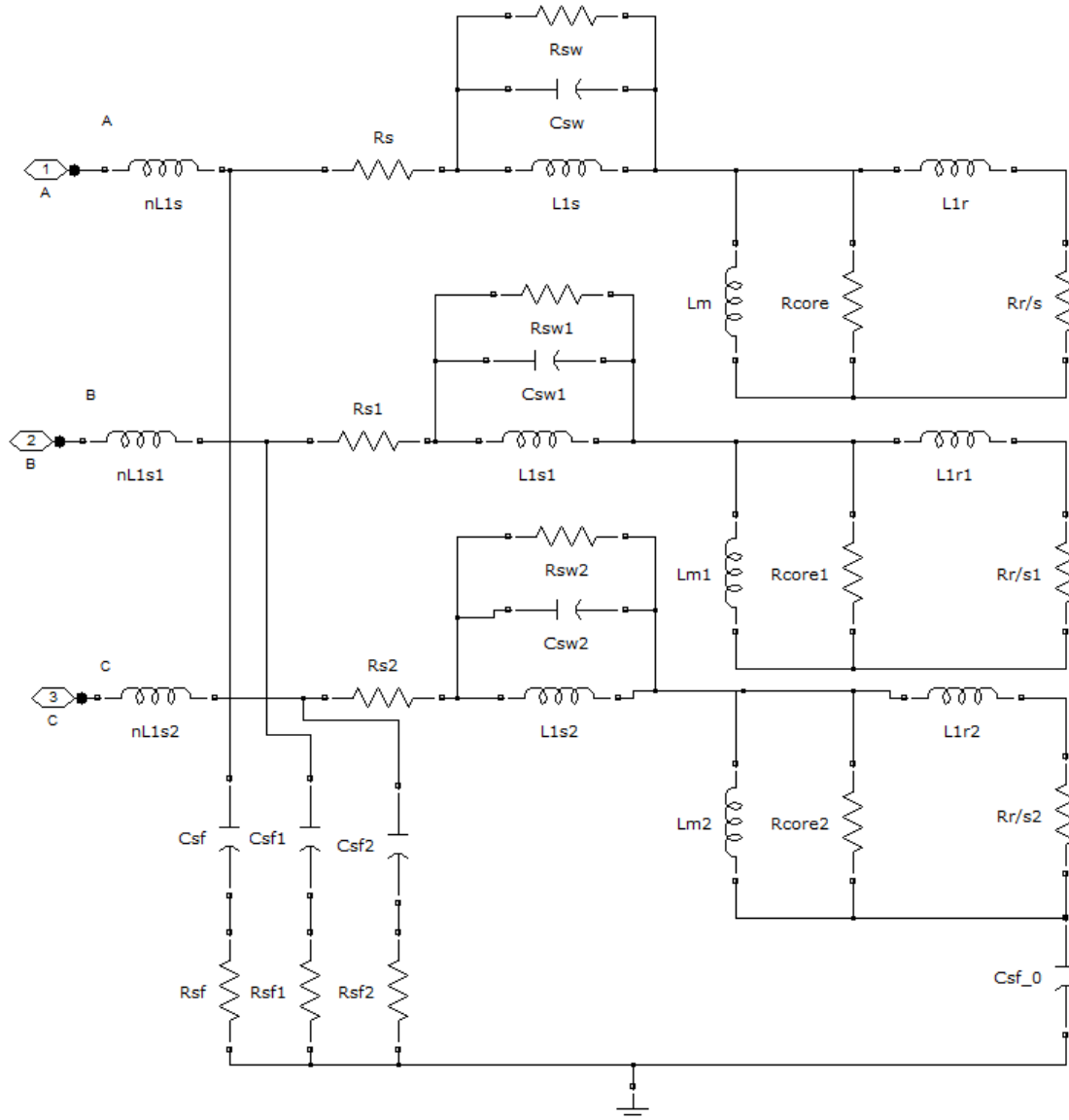


Fig. 5.6 Three-Phase Universal Motor Model

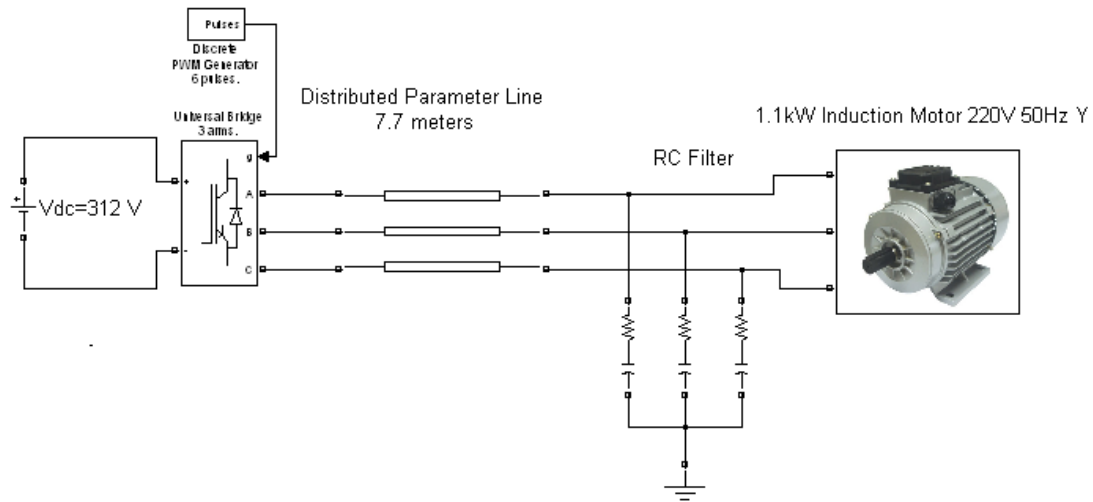


Fig. 5.7 Matlab Simulink™ Model of the System

From the simulation, the line-to-line voltage at the motor terminals is shown and the influence of the rise time T_r , the cable length l_c and filter application is also presented. The DC-bus voltage is 312V and the switching frequency is 1080Hz. The simulation runs for 0.01s in order to have several pulses from the PWM driven inverter.

The filter used in this chapter is calculated by equations (5.5) and (5.8), has fixed parameters in order to evaluate the effectiveness of a single designed filter. The filter capacitance was set with 0.1 μ s rise time and turns out to be 16 nF with $R_f = 58\Omega$.

Case $T_r = 0.1 \mu$ s, $l_c = 10$ m, without filter

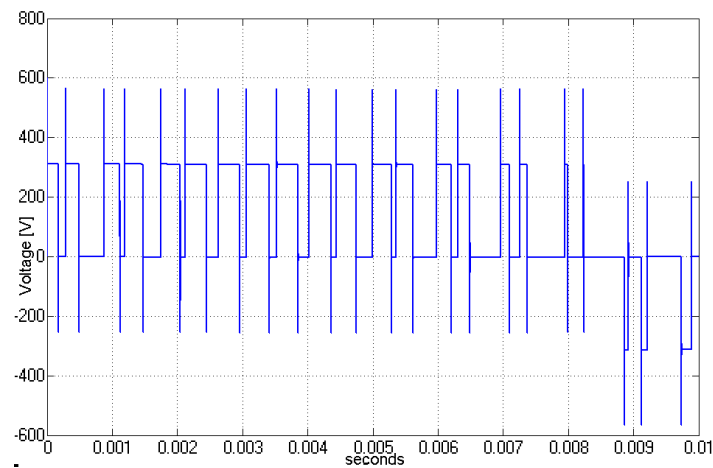


Fig. 5.8 Case A Line-to-line voltage with $T_r = 0.1 \mu$ s; $l_c = 10$ m; without filter

The line-to-line voltage at the motor terminals is shown in Fig. 5.8. The overvoltage on the line due to the reflection effect caused by the very short rise time of the square voltage at the inverter output is well visible.

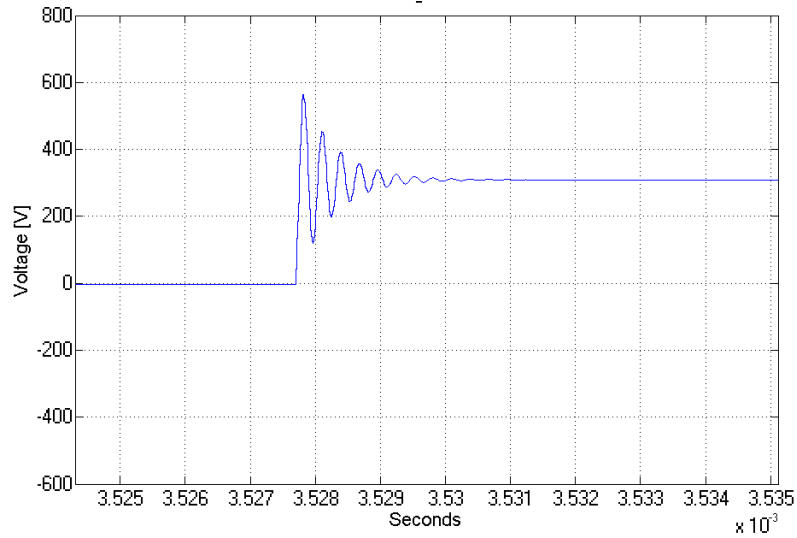


Fig. 5.9 Overvoltage zoom case A

An insight look at one of the voltage peaks is given in Fig. 5.9. The peak value reaches 563V which means an overvoltage factor $k = 563/312 = 1.8$

Thus the voltage is the 80% more compared to the DC-bus voltage.

Case $Tr=0.1 \mu s$, $l_c = 10m$, with filter

The effectiveness of application of the RC motor terminal filter, is illustrated in Fig. 5.10.

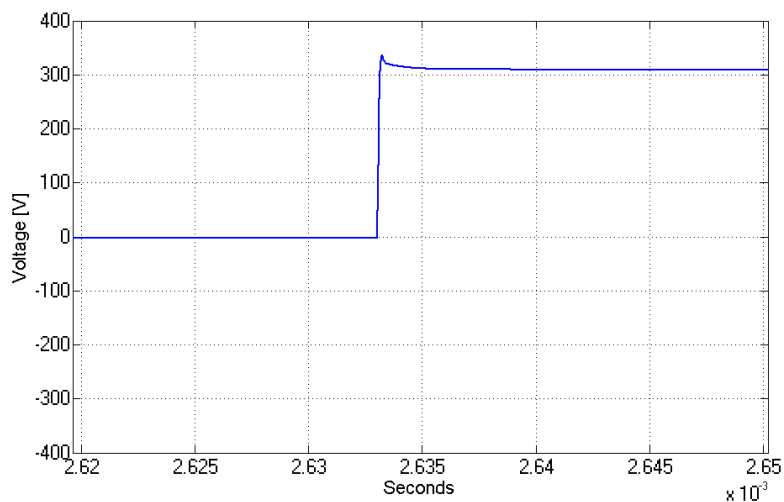


Fig. 5.10 Case B Line-to-line voltage zoom with $Tr = 0.1 \mu s$; $l_c = 10m$; with filter

With the same cable length and the same rise time, the overvoltage is strongly reduced.

In this case the voltage peak reaches only 337V that means $k = 337/312 = 1.08$. The voltage oscillation is no more present.

The increasing of the voltage rise time at the inverter output is expected to reduce the overvoltage at the motor terminals according to the previous studies [43]-[35]-[10]-[45] as the steep front of the voltage becomes less “severe”. This increment of rise time is just to demonstrate the reduction of the overvoltage on the simulation, but does not mean practical intervention on the gate resistance on physical IGBT; that would bring undesirable reverse recovery effects and increased losses problems [47].

In Table 5.3 other results from the simulation without the filter for different rise time, are presented.

TABLE 5.3
OVERVOLTAGE FACTOR FOR DIFFERENT RISE TIME

Tr [μ s]	0,1	0,2	0,4	0,7	1	1,5
$k = V_{overvoltage}/V_{dc}$	1.8	1.38	1.18	1.10	1.06	1.04

Now the effect of different cable length is investigated. As reported in all the studies concerning motor overvoltage from PWM feeding [43]-[35]-[10], the longer the cable, the nearer the overvoltage is to $2 \cdot V_{DC,bus}$ value.

Other overvoltage factors for different cable lengths are presented in Table 5.4 with $Tr = 0.1\mu$ s and without the filter.

TABLE 5.4
OVERVOLTAGE FACTOR FOR DIFFERENT CABLE LENGTH

lc [m]	5	10	15	20	30	40
$k = V_{overvoltage}/V_{dc}$	1,39	1,8	1,92	1,94	1,94	1,94

As expected, from 15 meters and over, the overvoltage factor is near to 2.

The influence of both, the rise time and the cable length is clearly shown in Fig.5.11.

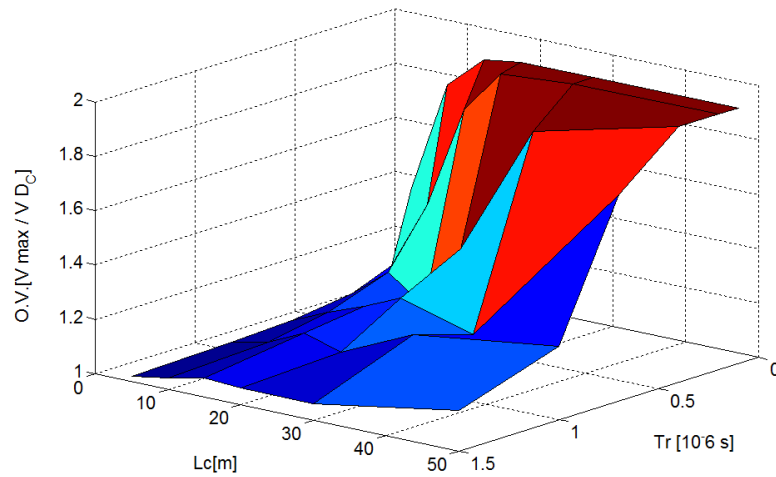


Fig. 5.11 Overvoltage factor on cable length and rise time

As the length of the cable increases beyond 15 meters and the rise time decreases under 0.4 μ s, the overvoltage factor nearly reaches 2. The voltage is almost double the DC-bus voltage, stressing the electrical insulation system of the machine every time a pulse occurs, and possibly causing severe damages to it.

5.6 Validation of Motor Model

To validate the construction of the Universal Motor model, experimental measurement has been derived and the comparison between the experimental data and simulation data is presented.

The induction motor is the one previously described.

The cable is the 4-conductors PVC Flexible, 7.7 meters long described in Section 5.2.1, and the inverter is the TOPVERT E1 manufactured by TOPTEK ELECTRONICS CORP. The measured impulse rise time T_r at the inverter terminals is 150 ns and the DC-Bus voltage is 312V.

A simulation of the model with $T_r = 150$ ns, $l_c = 7.7$ m and the proposed motor model is performed in order to compare the simulated results with the experimental one in the same condition.

The simulated and the experimental voltage measurements are presented in Fig. 5.12 and Fig. 5.13 respectively:

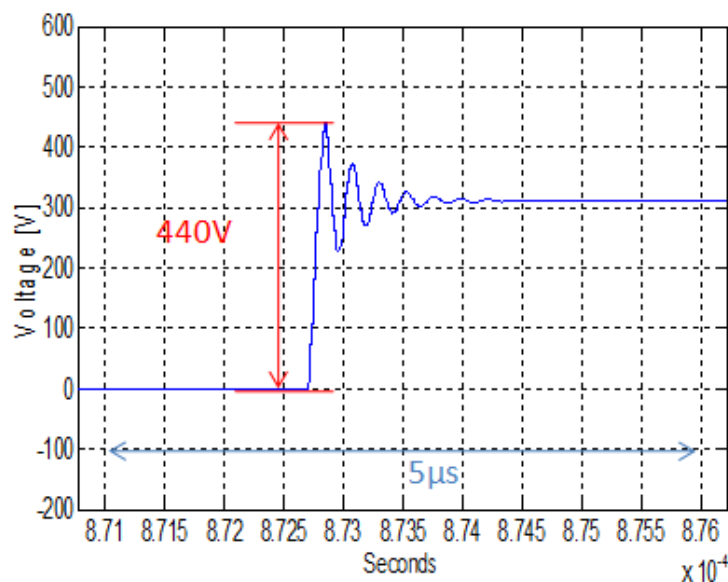


Fig. 5.12 Overvoltage from simulation

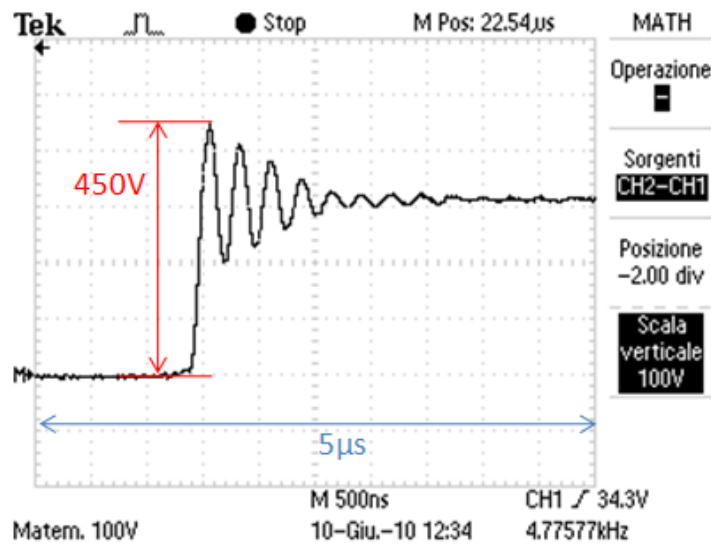


Fig. 5.13 Overvoltage from motor measurement

Figures shows that the voltage attenuation is a little different: that's because the Distributed Parameters Line does not represent precisely the frequency dependence of RLC parameters of real power lines as for the skin effect. The Simulink™ model results in a more attenuated voltage response to the inverter output voltage. Despite of that, the overvoltage levels match very well. The measured overvoltage is 450V and the simulated one is 440V, thus only the 2.2% less.

5.7 Conclusions

The results obtained from the simulation of a power system composed by an inverter model, cable model, RC filter and motor model are presented. The results well respect the previous analysis made on similar systems concerning the variation of overvoltage at motor terminals with respect to the cable length and to the voltage rise time at the inverter output. That means that the new universal induction motor model applied in a simulation environment of a power system gives good results and can be used for overvoltage prediction and filter dimensioning of a given system.

The motor model is built not only from circuit analysis, but also from impedance measurement to best match the experimental data with the model response. This fact guarantees the truth of the model results.

The validation of the motor model is also presented through the comparison between simulated and measured voltage response in the same condition. Data has been valued to be in a good agreement meaning that the motor model together with the cable model, well represent real situations in a inverter through-cable-fed induction motor.

Chapter VI: Case Study 2. On line Partial Discharges Test on Rotating Machines Supplied by IFDs

An on line partial discharge test technique on rotating machines fed by inverters is analyzed in this chapter. All the research to determine the configuration of the components was developed using simulation in Matlab SimulinkTM. The important fact is that the entire model was made with all the components and situations that result from partial discharges on the insulation of electrical rotating machines. The model of the rotating machine is in high frequency because it is fed by an inverter in order to visualize the overvoltage and partial discharge phenomena. Voltage impulse and partial discharge pulse spectra is filtering by a multipole filter before be passed through a coupling capacitor, connected to the machine terminals. Interesting results are showing in this chapter to verify the accuracy of this online partial discharge testing technique. Another objective is to find out the values of components parameters before to be implemented.

6.1 Introduction

Overvoltage phenomena in the insulation of rotating machines appear when such are fed by inverters. One of the causes for overvoltage is the fast switching of the insulated gate bipolar transistor included inside the inverter. When the PWM is generated, the rise time and the high frequency of operation are present. Thus the whole system operates in high frequency impedance, called surge impedance. A fed cable between the inverter and the machine is installed; often times this cable is long due to the physical separation between the machine and the inverter. The cable is operating in surge impedance because of the high frequency spectra of the electrical quantities. At the same time the rotating machine is operating in surge impedance by the same reason as before. When the first impulse travels through the cable at the velocity of 150-200 meters per microsecond, it arrives to the machine and sees a mismatch of surge impedance between the cable and machine. When this occurs, a reflection phenomenon is present, taken back 90 percent of the wave toward the inverter. At the same time the signal travels back to the machine terminals with higher amplitude, which could increase up to 90 percent. The wave reflected to the inverter comes back again to the machine terminals but with a negative value. When it arrives, it is reflected again and so on [17]. The analysis of this behavior permits to assert that the lengths of the cable and rise time are important factors that determine the overvoltage at the terminal machine [44].

When overvoltage is present at the machine terminal, electrical stress in the interturn insulation and core insulation is also present; this causes aging of the general machine insulation, increasing of the dielectric loss and causing partial discharge. If partial discharge occurs at high repetitive rate, it becomes a total destruction of the insulation, damaging and taking out of service the rotating machine, increasing the cost of operation of the plant [48].

On-line partial discharge testing has a strong advantage upon offline partial discharge test, in that it is possible to test the machines without taking them out of service, which can create an economic impact due to interrupted production. Thus the machine can be stopped just when necessary to perform preventive or corrective maintenance. It is known that the cost of offline testing is lower than online testing, but that initial cost is fully recovered by means of

economical saving from the advantage. With this plan it is possible to avoid the total destruction on the insulation and windings. The simulation tool presented in this thesis is a valid instrument to predict the parameters of the elements of the configuration proposed by [9] analyzed in this chapter.

The simulation presented in this paper is accurate and the evidence is mainly the complexity of the element models. For example, the machine model was designed especially for the analysis in high frequency, took into account the behavior of the insulation hence the impedances and capacitive effects between windings and verified through experiments by [28]. According to [45]-[43] the rise time can be extended incorporating an inductor filter at the inverter terminal, this way the overvoltage at the machine terminals is reduced and minimizes the partial discharge Inception voltage (PDIV). Also the scope results prove this model to be accurate, where it shows reduced overvoltage and PDIV because of the incorporation of the filter at the inverter terminals. All of this is just the setup of a variable system, to start to check the good response of our measurement configuration of partial discharge pulses.

The online PD measurement technique used in this paper is based on a coupling capacitor sensor in series with a resistor connected to ground on a filter that suppresses the electrical noise from the power system. The capacitor has a voltage exceeding the expected applied impulse voltage, because it is connected to the machine terminals. The measurement is read by an oscilloscope or an analyzer connected in parallel with a resistor in series with the partial discharge sensor [49]-[50]-[9]. The Fig. 6.1, shows the configuration.

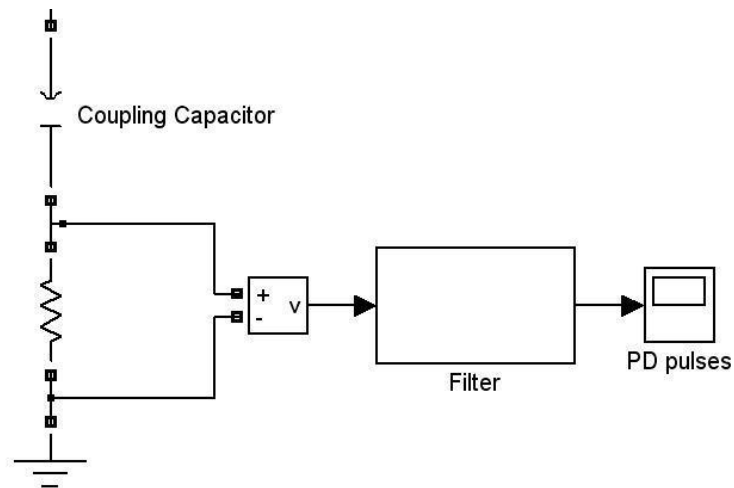


Fig. 6.1 On Line partial discharge test configuration

6.2 Simulation Components

6.2.1 Application of Cable Model

An accurate cable model is necessary to represent the behavior of the overvoltage phenomena and to allow a good analysis of the lead in high frequency. This model of cable was analyzed checking the frequency response of the power cable characteristic impedance developed by [45].

The cable characteristic impedance is calculated from short to open circuit impedances over a broad range of frequency. The cable model series parameters are associated to the behavior of the short-circuit impedance, while the parallel parameters are associated to the behavior of the open-circuit impedances [45]: the model is shown in Fig. 6.2.

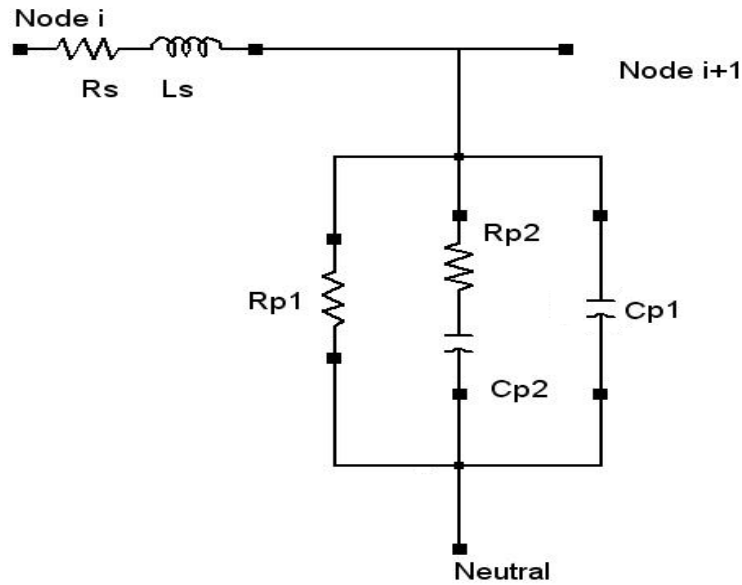


Fig. 6.2 High Frequency Cable model [45]

TABLE 6.1
EXAMPLE OF PARAMETERS OF HIGH-FREQUENCY MODEL OF TWO DIFFERENT CABLE GAUGES
FROM [45]

Cable Gauge	R_s (m Ω)	L_s (μ H)	R_{p1} (M Ω)	R_{p2} (k Ω)	C_{p1} (pF)	C_{p2} (pF)
6	1.5	0.24	173.9	13.9	137.1	22.5
14	16.0	0.29	265.7	25.4	93.7	16.8

*Length of samples cable, 1 meter

6.2.2 Used Rotating Machine Model

In this case, in order to complete a good entire model, for the measurement of partial discharge it is important to use a model machine that accomplishes the requirement of high frequency behavior, taking into account the impact of magnetic core, parasitic interturn, winding to frame capacitors, and skin effects of windings.

In [28] the authors introduce analytical equations and resonance points in a measured common mode and differential mode impedance versus frequency test. This model has an impedance response at low to high frequencies up to 10MHz very close to the differential mode and common mode measurement on a 100HP 460V-Delta, 60Hz induction motor. These results prove that this model is very useful to the study of reflected wave and overvoltage phenomena [28].

6.3 On line PD Test Components

6.3.1 General

High-voltage capacitors installed on each phase terminal are very popular. A widespread solution is also the high-frequency current transformer (HFCT), and the bandwidth is from 100kHz to 30MHz, with a 50Ω load. Another alternative is Electromagnetic couplers, antenna type couplers. These entire sensors are sensitive to the high-frequency signal from the partial discharge, from tens of kHz to 1GHz. Filtering techniques to process the sensor signal are able to optimize the information and to separate electrical noise from partial discharge pulse [50].

In offline and online partial discharge testing the coupling capacitor blocks the power frequency 60Hz, while serving as a low-impedance path for the high-frequency partial discharge pulses [50].

When partial discharge inception voltage (PDIV) is reached, partial discharge occurs according to the voltage of the switching function from the inverter and repetition rate level [51]. By definition, PDIV is the lowest voltage at which partial discharges occurs, continuously, above some stated magnitude [9].

6.3.2 Settings

Several different parameters may influence the configuration for the online partial discharge testing. In this chapter the coupling capacitor sensor will be studied.

The model and parameters of the 100HP 460V-Delta, 60Hz induction motor on [28] is used, while the power cable model reported on [45] is considered. The authors of this paper made measurements with a RLC bridge of a 3AWG cable to reach the parameters, because of the power machine.

The partial discharge sensor is connected to the terminal of the machine with all the nominal parameters.

The coupling capacitor is set according to a high sensibility behavior, since the 500pF capacitor can detect some partial discharges pulses while the 80pF capacitor is not sensitive enough [49]; in the simulations the sensor will be 500pF or 80pF connected to ground through a resistance with a value between 10Ω to 500Ω [9].

The filtering techniques can be active or passive technologies, with a high-pass filter, such cutoff frequency ranges from about 10kHz to about 5MHz. Finally the signal after the filter is displayed on a scope of the simulation, while in the real plant may be shown in an oscilloscope, pulse height analyzer or pulse phase analyzer [9].

6.4 Simulation Results

The model simulation was built according to the diagram on Fig.6.3. The parameters of the cable are equivalent to 30m in length, 3AWG. The model parameters are $R_s=0.5m\Omega$, $L_s=0.22\mu H$, $R_{p1}=148.1M\Omega$, $R_{p2}=6.1k\Omega$, $C_{p1}=151.2pF$, $C_{p2}=26.3pF$, per meter. The motor was set according to the model and parameters from reference [28]. The inverter is 3 bridge arms, discrete PWM generator 6 pulses at 60Hz, two levels, DC bus 650V, since the motor is 460V, and rise and fall time 100 ns. The online test components values are, coupling capacitor 500pF, Resistor 40Ω , and 2nd-Order high-pass filter cutoff frequency 2MHz.

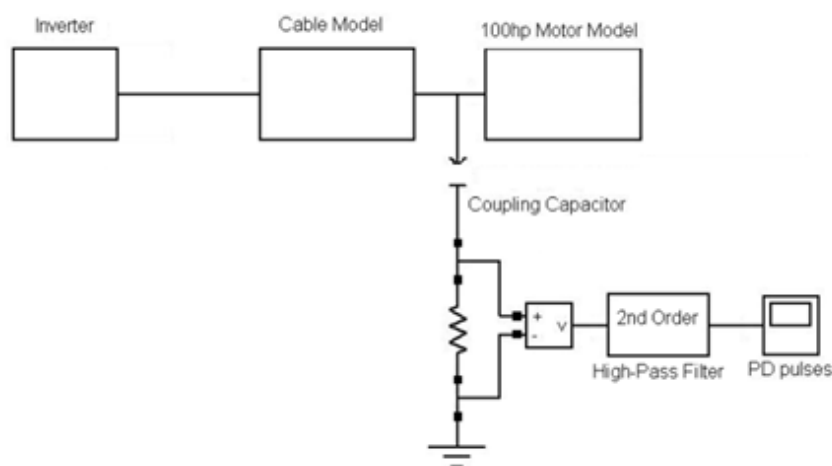


Fig. 6.3 Block Diagram of Simulation On-Line partial Discharge test with Coupling Capacitor (rise time 100 ns)

The inverter generates a square wave with very short rise time, which is one of the principal causes of overvoltage on terminal machines [44]. The shorter is the rise time, the highest the Overvoltage and Partial Discharge Inception Voltage. That is how the PDIV is generated on the machine model, because in machine model the dielectric resistance, capacitive effects of the insulation between windings are considered. The motor model response was validated by the experimentation performed by the authors on [28].

The first simulation is realized with a rise time of 100 ns as shown in Fig.6.3. The scope results are Fig.6.4, and Fig. 6.5, shown the normal square signal in the inverter output, and the overvoltage on the machine terminals, respectively.

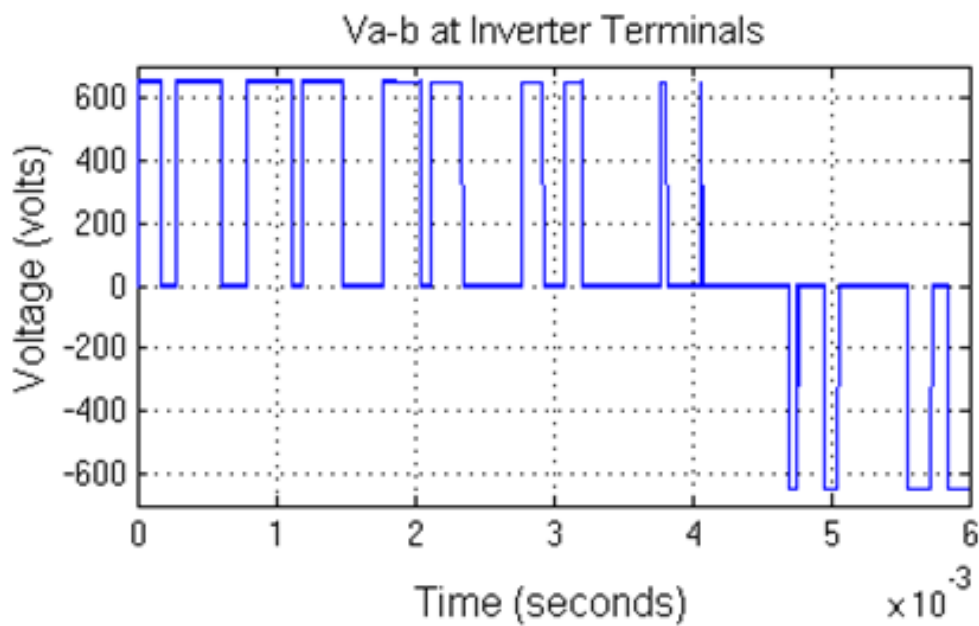


Fig. 6.4 Pulses at the inverter terminals rise time 100 ns

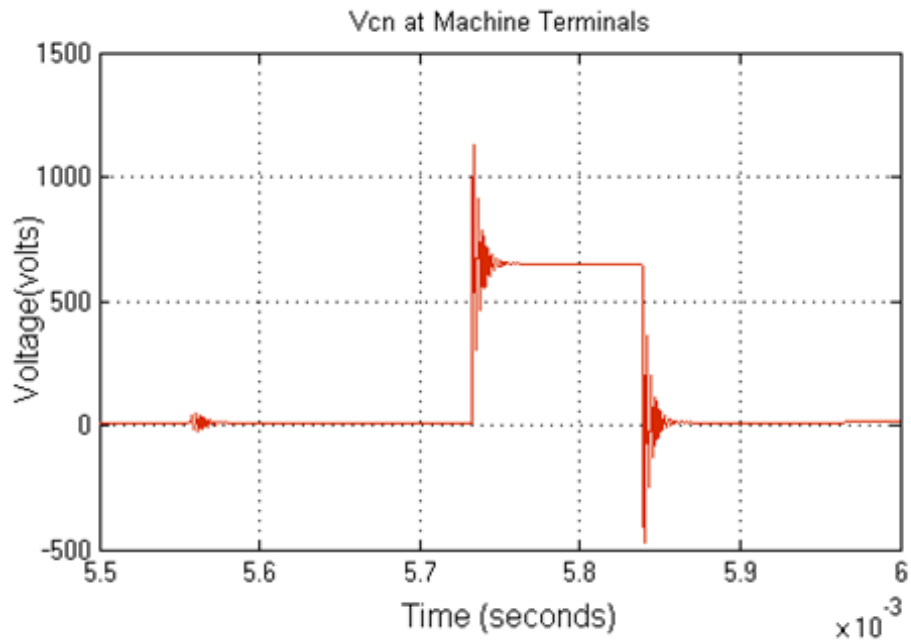


Fig. 6.5 Overvoltage on motor terminals rise time 100 ns

The overvoltage reaches 1100V, or 450V over DC bus, this is the target situation to perform the online PDIV measurement.

At the scope of PD test the simulation shows three PDIV in the same place at the time of the commutation of the inverter, fall time 5.84 ms, rise time 5.73 ms, and rise time from the other winding phase group transmitted by induction at 5.55 ms Fig.6.

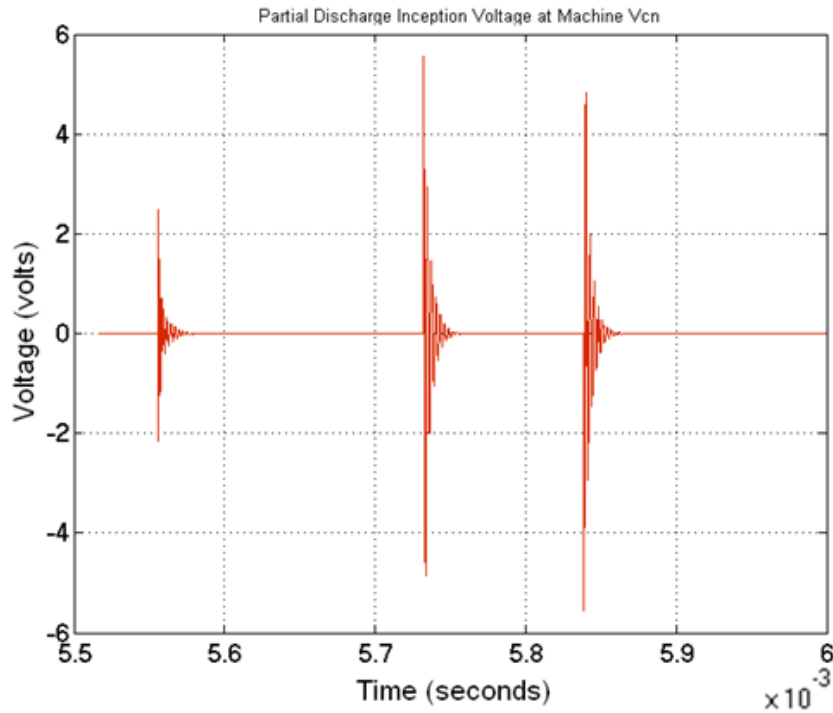


Fig. 6.6 Partial Discharge Inception Pulse at the commutation of inverter with rise time equal to 100 ns

A Reactor Inverter Output 2nd-Order Low-pass Filter Fig.6.7, is connected between the inverter and cable Fig.6.8, thus the rise time is prolonged to 2 μ s, and the overvoltage is reduced [43] Fig.6.9, as a consequence, the Partial Discharge Inception Pulse is also reduced Fig.6.10.

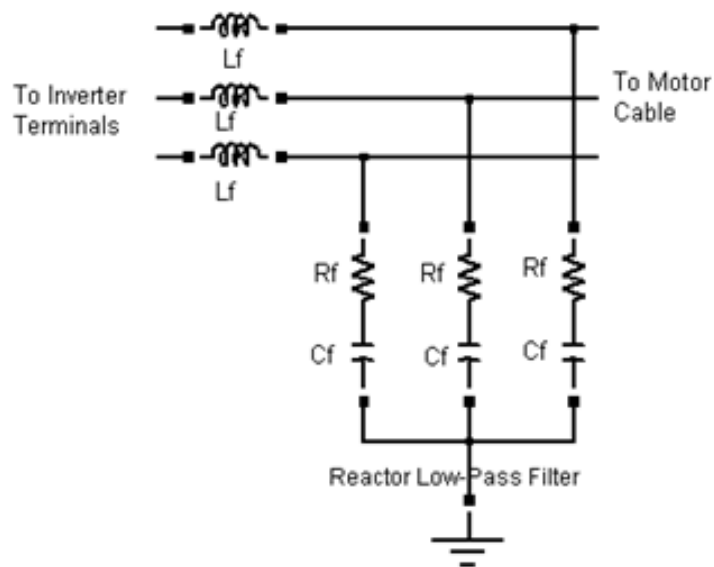


Fig. 6.7 Second Order Low-pass Filter

Using the design criteria reported on [43], the inverter output filter values in this case are $R_f=60\Omega$, $L_f=0.0925\text{mH}$, $C_f=0.10279\mu\text{F}$.

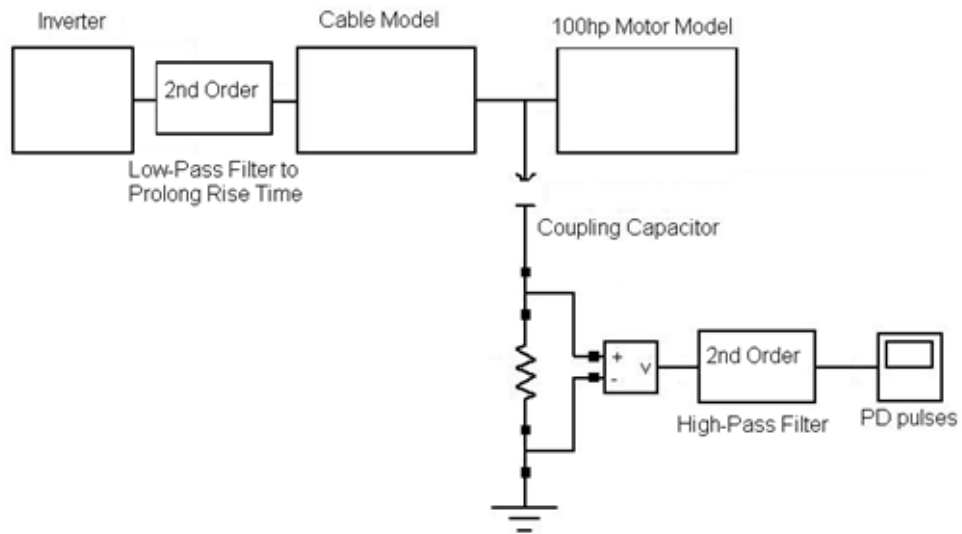


Fig. 6.8 Block Diagram of Simulation On-Line partial Discharge test with Coupling Capacitor and inverter output reactor filter (rise time $2\mu\text{s}$)

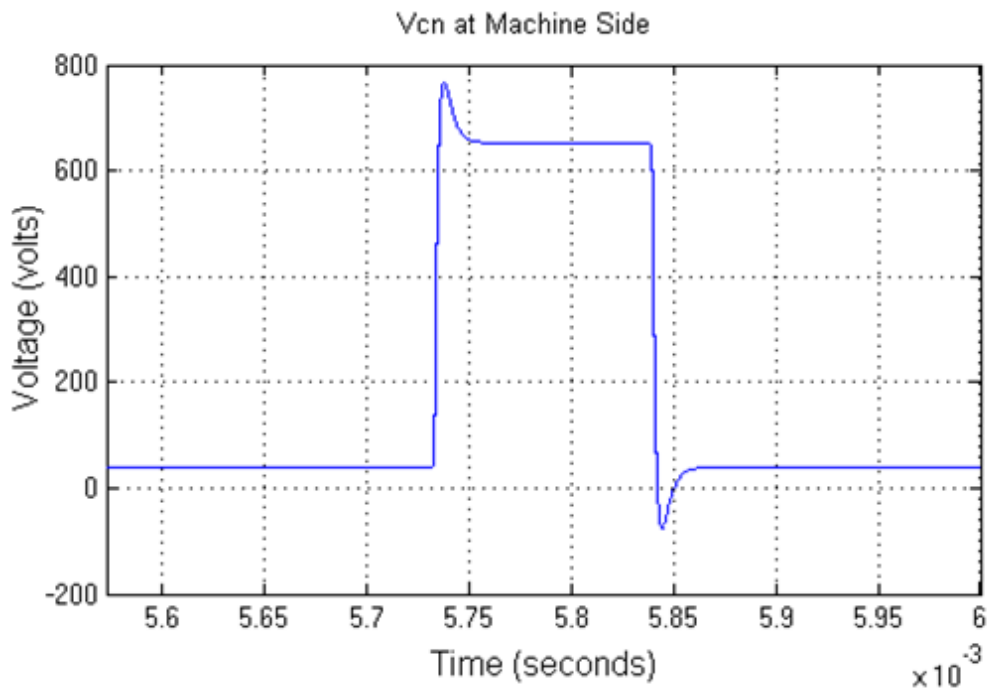


Fig. 6.9 Overvoltage on motor terminals with low pass inverter output filter

At this time the overvoltage reaches 750V or 100V above of DC bus voltage. The low-pass filter increments the rise time of pulse downstream, hence not in switch device, in that way undesirable reverse recovery effects are avoided.

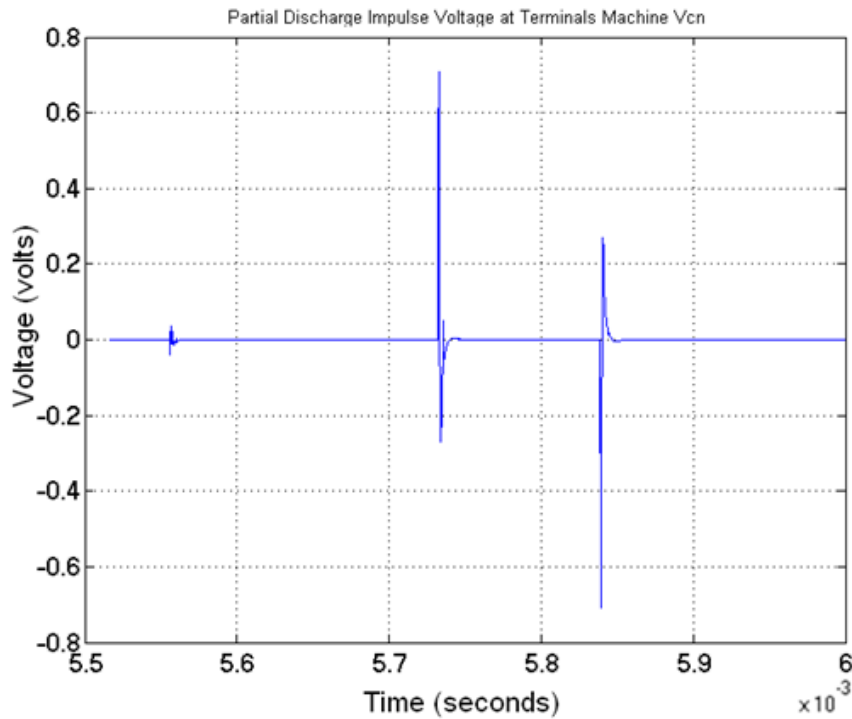


Fig. 6.10 Partial discharge inception voltage at the commutation of inverter with low-pass inverter output filter

And again the PDIV is shown at the same time of the commutation from the PWM Fig.6.9, it shows a direct relationship between them. At the rise time 5.73 ms, the PDIV is 708mV.

6.5 Conclusions

The overvoltage and the partial discharge inception voltage are due to the length of cable and rise and fall time from the inverter PWM.

The PDIV are concentrated at the rise and fall time of the modulation. At the same time the partial discharge pulses induce in the nearest windings some disturbances, as shown in Fig.6.6, and Fig.6.10, at time 5.55 ms a distortion can be observed.

Partial discharge creates small pulse currents that travel along the stator winding; the sensor (coupling capacitor) is able to capture these currents. It is well known that the closer the sensor is to the winding, the better the measurement will be; for that reason the model verifies the actual standards.

The installation of the of 2nd Order low-pass inverter output filter, increased the rise time, then decreased the overvoltage and partial discharge inception voltage (PDIV), verified by Fig. 6.10, 708mV with rise time of 2 μ s, which is less voltage than 5561mV with rise time of 100 ns Fig.6.6.

This configuration of the online PDIV test has enough accuracy due to the clear results. The setting of the multi-pole filter must be flexible in terms of cutoff frequency because the parameters of every machine and inverter are different case by case. The value of the resistor between the coupling capacitor and earth must be the lowest possible value in order to see the currents impulses that are traveling through the system.

Chapter VII: Back to Back Converter

7.1 Inverter Control

7.1.2 Three Phase Grid Side Converter Control

This control is designed to ensure the maximum active power flow from the machine towards the grid, and it also maintains the DC Link voltage constant.

$$U_d = -U_{id} - R_g i_d - L_g \frac{di_d}{dt} + \omega L_g i_q \quad (7.1)$$

$$U_q = -U_{iq} - R_g i_q - L_g \frac{di_q}{dt} - \omega L_g i_d \quad (7.2)$$

Equations (7.1) and (7.2) represent the grid model connection, where the reference frame is oriented along the grid d-axis, L_g and R_g are the inductance and resistance in the grid connection respectively [52], as illustrated in Fig.8.2.

The d-axis of this control regulates the DC-Link voltage using the error between V_{dc}^{ref} and, V_{dc}^{mea} which is processed by the PID controller with anti-wind up. Thus the active power is transmitted from the rectified (SSC) to the grid through the inverter (GSC).

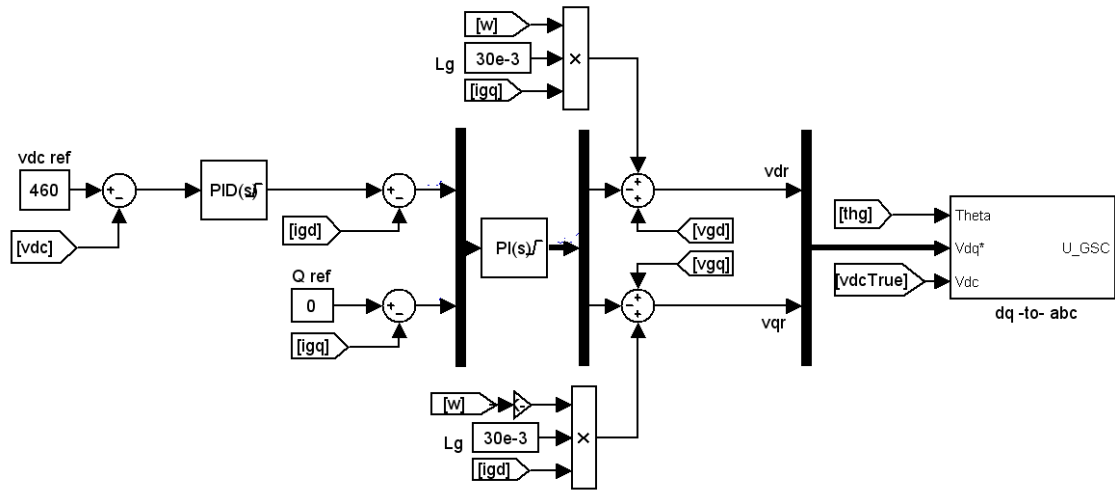


Fig. 7.1 Three Phase Grid Side Converter Control

Compensator components are placed on the d-axis control and q-axis control, with the product values of ω frequency from PLL output, and L_g grid inductance connection. These compensators have to exchange the information i_d and i_q from grid in order to decouple the currents.

In this case the reactive power reference is zero, and therefore the goal of the i_q controller, is to accomplish that requirement. Obtaining the error between $i_q^{ref} = 0$ and measured quadrature current on the grid, i_q^{mea} is regulated by a PI controller. The quadrature component of the grid voltage is added with the compensator component and the result is subtracted from the voltage suggested by the PI controller.

The d-axis voltage reference is divided by V_{dc} as given in equation (7.3), to obtain the required value for modulation.

In order to obtain the values of V_{abc} a similar modulator used in SSC with an anti-transformation $d - q/abc$ is used.

$$m = \frac{v_d}{V_{dc}} \quad (7.3)$$

7.2 Stator Side Converter Control

The Stator Side Converter, is controlled in such a way that $isd^{ref} = 0$, and isq is able to induce sufficient electromechanical torque (Te), to obtain the desired speed on the machine. The differential equations for the machine control are shown below:

$$Usd = Rs isd + Ls \frac{d}{dt} isd - \omega_e Ls isq \quad (7.7)$$

$$Usq = Rs isq + Ls \frac{d}{dt} isq + \omega_e \psi_{pm} + \omega_e Ls isd \quad (7.8)$$

To control the velocity of rotor, the mechanical speed, ω_m on the shaft is measured, and multiplied by npp to obtain ω_e . The value ω_e in rad/s is compared with ω_e^{ref} . Then a PI controller performs the task to obtain the (Te) reference torque. isq reference is then found using the following equation.

$$isq^{ref} = \frac{Te}{npp * \psi_{pm}} \quad (7.9)$$

Where:

npp Pairs machine poles.

ψ_{pm} Flux Linkage Permanent Magnets.

The isq^{ref} signal is compared with the actual isq , and the error is processed by another PI controller to obtain Vsq^{ref} . To this Vsq^{ref} are added the last term in equation (7.8), coupling compensator term and, the motional electromotive force show in equation (7.10).

$$\varepsilon = \omega_e * \psi_{pm} \quad (7.10)$$

The d-axis reference of current control is set to zero, and it is compared with the measured isd from the winding of the machine, and then it is controlled by a PI controller to achieve Vsd^{ref} . To avoid unwanted affects when the machine is starting from a velocity different from zero, it is necessary to add coupling compensator term, which is the last term in equation (7.7).

The switching functions $Vabc$ are built sinusoidal and balanced by the mean of Park component Vd, Vq with an anti-transformation $d - q/abc$ driven by the PLL (Phase Locked Loop) output phase signal.

These switching functions are passed through a PWM Generator 2 level type, commuted device IGBT, with carrier frequency equal to 10 kHz.

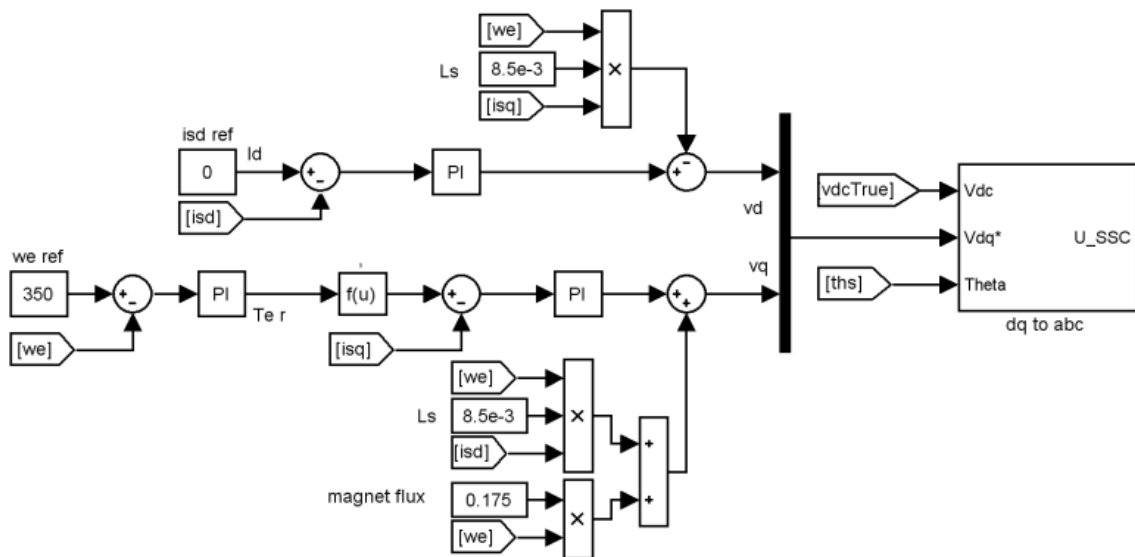


Fig. 7.3 Stator Side Converter Control

In Fig. 7.3 it can be seen that $isd^{ref} = 0$. The theta angle (ths) is obtained from rotor angle measurement in radians.

Chapter VIII: Case Study 3. Control for Grid connected PMSG Wind Turbine with DC Link Capacitance Reduction

An enhanced control is presented that effectively cancels the noise in torque, and currents in a wind turbine Permanent Magnet Synchronous Generator. The proposed control also allows the reduction of the DC-Link capacitance. Simulations succeed on Three-Phase and Single-Phase grid connection, through a Back to Back converter. The grid side converter switching function was modified with an algorithm that represents the noise from grid frequency. The DC Link ripple due to capacitor reduction was canceled, and as a consequence there were no noise frequencies on electromagnetic torque, stator and grid currents after the algorithm was implemented. Remarkable reduction in DC Link capacitor was possible, making the system more reliable and economical. The PMSG is protected from core saturation, because stator currents consist of only the fundamental frequency component. This results in a constant torque, preventing mechanical stress.

There are several machines that are used for electrical power generation from wind energy. One of the most used in the market is Permanent Magnet Synchronous Generator (PMSG), because of its high efficiency and reliability. The trend in the case of wind power systems is the development of large wind turbines up to 6MW on wind farms. On the other hand, small scale wind power system configurations are applied to isolated areas such as rural sectors and small islands away from big cities [53].

The use of permanent magnets on electrical machines is often more economic and efficient, due to the magnetic material improvements [54].

A control for PMSG connected to the grid through a back to back converter is presented. The PMSG has a three phase wound stator. Normally there is a large capacitance in the DC Link in this kind of configuration, due to the need to buffer pulsating power from the grid especially in the case of single phase grid connection.

The solution presented in this work shows excellent results for both three and single phase grid system with a smaller DC-Link capacitor.

Although there is one recent paper, pointing to the capacitance reduction in a single phase grid connection [55], this chapter proposes a more efficient solution, since it corrects DC-link ripple as well as the torque and grid current and stator currents. This is possible considering V_{dc} error information as the correcting factor, thus considering the double grid frequency component and ripple due to commutations of IGBT switches. This solution is applicable for both three-phase and single-phase grid connection. With the proposed solution in effect the capacitor in the DC Link can be reduced several times, thus making the system more reliable and economic.

Moreover the switching frequency harmonics appearing in the stator current is compensated. Since the presence of switching frequency harmonics in the stator current is responsible for generating the undesired torque pulsations in the electromagnetic torque T_e the proposed solution is able to prevent torque pulsations.

Finally, optimizing the control of d-axis and q-axis on stator currents, copper and core losses, can be minimized.

The two configurations and its solutions are simulated on Matlab SimulinkTM software, as shown in Fig.8.1 and Fig.8.2.

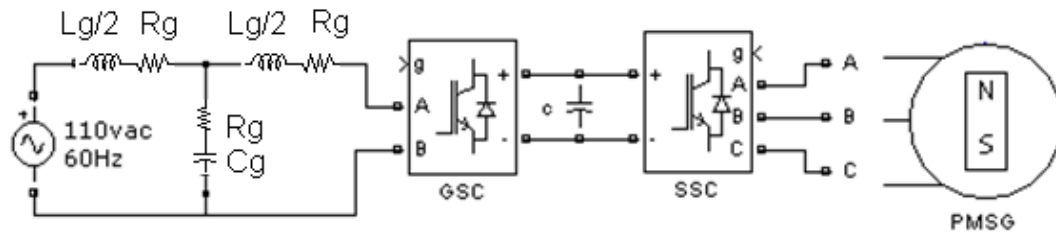


Fig. 8.1 PMSG connected to the Single Phase Grid through back to back converter

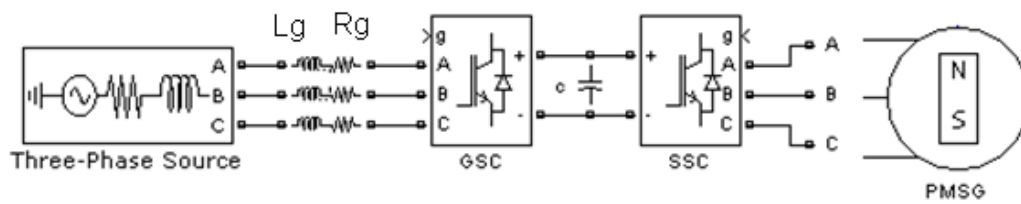


Fig. 8.2 PMSG connected to the Three Phase Grid through back to back converter

8.2 Parameters of Permanent Magnets Synchronous Machine

TABLE 8.1
PARAMETERS OF THE MACHINE

Number of phases	3
Nominal Power (W)	1100
Rotor type	Salient-pole
Mechanical input	Torque T_m
Stator phase resistance R_s (ohm)	2.875
Inductances [L_d (H) L_q (H)]	[8.5e-3, 8.5e-3]
Flux linkage permanent magnets (V.s)	0.175
Machine poles (np)	4
Frequency (Hz)	60
Voltage Line to Neutral (V)	110

The above mentioned control and the machine parameters given in TABLE 8.1 are used in the case of both, Three Phase and Single Phase grid connections.

8.3 New Implementation of Algorithm on Wind Energy

The necessity to minimize the ripple on grid currents, rotor currents and, electromagnetic torque is an important aspect, to search for a reliable solution to this issue. Since the switching frequency in PWM generators and double grid frequency from single phase grid are the responsible of those harmonics. The proposed solution is implemented in the GSC switching function before the PWM generator. Significant harmonic frequency was observed in the DC-Link, and as a consequence a pulsation on currents and electromagnetic torque T_e . The undesired torque pulsation result in additional core losses [56]-[57].

A constant DC Link voltage can be obtained by using large DC Link filter, but these filters have disadvantages of being bulky, unreliable and they also contribute in slowing the response increasing time and also cost and losses [58].

8.3.1 The proposed Solution

The following technique can be applied to three-phase and single-phase DC-AC converters. The PWM control signals are generated by comparing the carrier signal and a reference signal as shown in (Fig.8.3.a-b). When there are noise frequencies on the DC Link, (Fig.8.3.c), it is possible to add that frequencies noise to the switching function, giving a *modified switching function*, (Fig.8.3.d). With the information of DC-Link error the switching function is modified. When the DC-link voltage differs from the reference value, the switching function is modified; thus compensating the error.

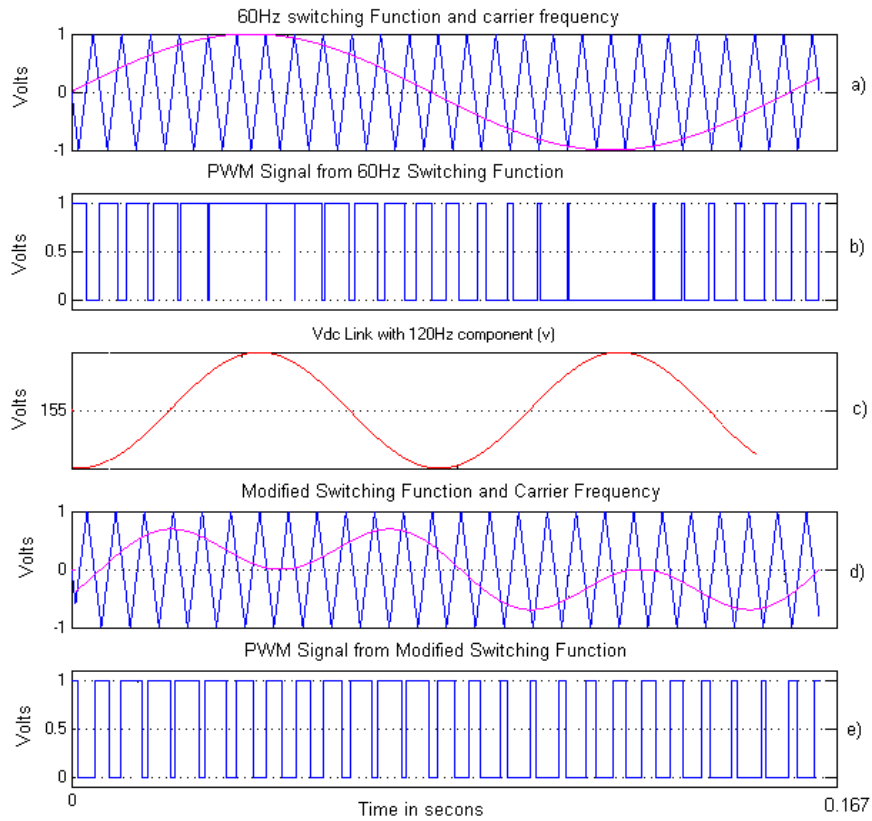


Fig. 8.3 Graphic draw of proposal as example

In this kind of control where V_{dc} is controlled by GSC the error on V_{dc} is corrected.

8.3.2 Demonstration

The switching functions for a three phase converter are:

$$SF_{3phase}(t) = [SF_{a1}(t) SF_{b1}(t) SF_{c1}(t)] \quad (8.1)$$

$$SF_{a1}(t) = \sum_{n=1}^{\infty} A_n \sin(n\omega t) \quad (8.2)$$

$$SF_{b1}(t) = SF_{a1}\left(\omega t - \frac{2\pi}{3}\right) \quad (8.3)$$

$$SF_{c1}(t) = SF_{a1}\left(\omega t + \frac{2\pi}{3}\right) \quad (8.4)$$

The lines to neutral voltage are expressed as:

$$[v_{ao}(t) v_{bo}(t) v_{co}(t)] = \frac{v_{dc}}{2} * [SF_{a1}(t) SF_{b1}(t) SF_{c1}(t)] \quad (8.5)$$

$$v_{ao \text{ without rip}}(t) = \frac{V_{dc}}{2} * SF_{a1}(t) \quad (8.6)$$

$$v_{ab \text{ without rip}}(t) = \frac{\sqrt{3} * V_{dc}}{2} * A_1 \sin(\omega t + \frac{\pi}{6}) \quad (8.7)$$

The magnitude of the fundamental output voltage, when the input is ripple free V_{dc} is given by $A_1 * (\sqrt{3} * V_{dc}/2)$ where A_1 is the magnitude of the fundamental component of the switching function.

In our Single-Phase and Three-Phase system grid connection originally the DC Link has a capacitor of $990\mu\text{F}$ and $500\mu\text{F}$ and, those will be reduced to $60\mu\text{F}$ and $35\mu\text{F}$, respectively. Now the DC Link voltage with ripple will be:

$$V_{dc \text{ with ripple}}(t) = V_{dc} + V_{\text{ripple}}(t) \quad (8.8)$$

$$V_{\text{ripple}}(t) = V_{dc} * K * \sin(\omega r * t) \quad (8.9)$$

If a second harmonic frequency from grid is present on DC-Link ripple, $V_{\text{ripple}}(t)$.

$$V_{dc \text{ with ripple}}(t) = V_{dc}(1 + K * \sin(2 * \omega * t)) \quad (8.10)$$

Then the algorithm which modifies the switching function to make the Grid Side Converter in this case, corrects the ripple on its input and output should be:

For Single Phase system:

$$SF_{1\text{phase mod}}(t) = \frac{1}{1+K*\sin(2*\omega*t)} * SF(t) \quad (8.11)$$

In Three Phase System:

$$SF_{3\text{ph}}(t) = [SF_{a1}(t) SF_{b1}(t) SF_{c1}(t)] \quad (8.12)$$

$$SF_{3\text{ph mod}}(t) = [SF_{a1 \text{ mod}}(t) SF_{b1 \text{ mod}}(t) SF_{c1 \text{ mod}}(t)] \quad (8.13)$$

$$SF_{3\text{ph mod}}(t) = \frac{1}{1+K*\sin(2*\omega*t)} * SF_{3\text{ph}}(t) \quad (8.14)$$

When this algorithm is implemented on three phase system, what occurs, for example, in one of the phases of a three-phase converter; is shown in the following expression without ripple:

$$V_{ao \text{ mod}}(t) = \frac{V_{dc \text{ with ripple}}(t)}{2} * SF_{a1 \text{ mod}}(t) \quad (8.15)$$

$$SF_{a1\ mod}(t) = \frac{1}{1+K*\sin(2*\omega*t)} * SF_{a1}(t) \quad (8.16)$$

$$V_{ao\ mod}(t) = \frac{v_{dc} * 1+K*\sin(2*\omega*t)}{2} * \frac{1}{1+K*\sin(2*\omega*t)} * SF_{a1}(t) \quad (8.17)$$

$$V_{ao\ mod}(t) = \frac{v_{dc}}{2} * SF_{a1}(t) \quad (8.18)$$

And the favorable result is the fact; that equation (8.18) is the same as equation (8.6).

$$V_{ao\ mod}(t) = v_{ao\ without\ rip}(t) \quad (8.19)$$

In this way we are able to cancel any harmonic frequency present on the DC Link, in order to have just the fundamental frequency at the output of our converter [59].

8.4 Simulations Results

The electromagnetic torque Te required by the PMSG to generate the nominal active power is:

$$Te = \frac{P}{\omega_e/n_{pp}} \quad (8.20)$$

Since in single phase system the rotor angular speed of reference is $\omega_e^{ref} = 350\ rad/s$ on Fig.7.3 and,

$$\omega_e = 2 * \pi * f \quad (8.21)$$

The currents frequency on stator are=55Hz, observable on (Fig.8.9.d) and (Fig.8.11.d). And the grid voltage frequency is 60Hz.

The switching function of GSC is modified according to equation (8.11) in single-phase grid connection and, equation (8.14) in three-phase grid connection.

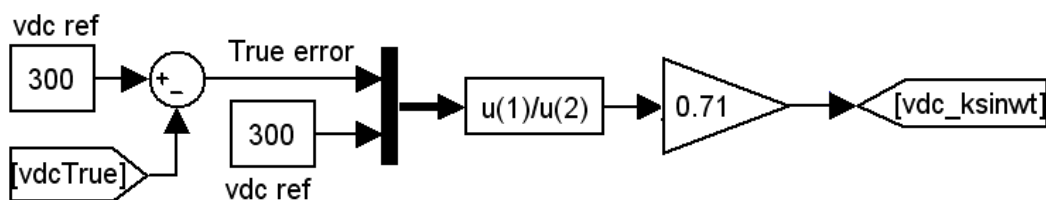


Fig. 8.4 V_{dc} error used as a correcting signal to modify switching function

The frequencies and amplitude errors on V_{dc} are used as the $k * \sin(wr * t)$ term for the proposed algorithm. In the case of single-phase connection, the most relevant second order harmonic from grid is included. Also harmonics with smaller amplitude are included, such as switching frequency harmonics.

From classic control of this kind of converters, the V_{dc} measured signal is filtered with a low pass filter before to obtain the error required by PID V_{dc} controller, but the others V_{dc} signals involved in this control should not be filtered: the not filtered signal is called $V_{dc True}$.

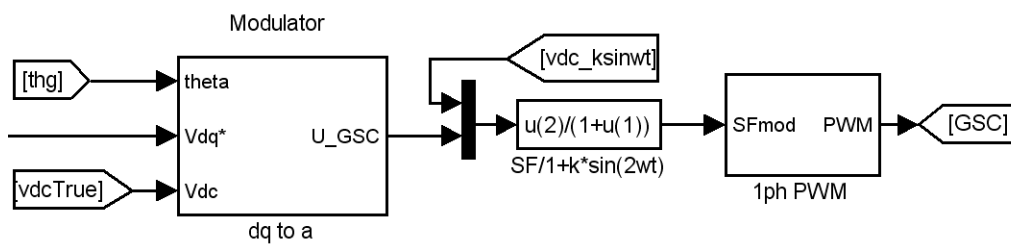


Fig. 8.5 Algorithm between Modulator and PWM Generator on GSC control

Fig.8.5 shows how this is incorporated to complete the algorithm that modifies the GSC switching function.

8.4.1 Connection to Three Phase Grid

This simulation is for the system shown in Fig.8.2. There is a LR filter at the converter output, just before it is connected to the grid.

On the initial state, the capacitance on the DC Link is $500\mu\text{F}$ which is favorable as shown in reference [52]. The simulation scope waveforms in Fig.8.6 show the current and torque waveforms without the algorithm in equation (8.9.5) implemented. It can be observed that there is no ripple in stator currents (Fig. 8.6.d) and, as a consequence electromagnetic torque is constant (Fig.8.6.c). The high value of capacitance on DC Link is helping, to maintain the DC-Link voltage V_{dc} constant and ripple free.

The capacitance is reduced to $35\mu\text{F}$ Fig.8.7. The DC-Link voltage shows a significant low frequency ripple component (Fig.8.7.b). It can also be observed that as a consequence the stator currents are distorted (Fig.8.7.d).

When the switching function is modified by the proposed algorithm in equation (8.14) it can be seen from the simulation waveforms in Fig. 8.8, that the stator currents are undistorted and the DC-bus voltage is ripple free even with a smaller DC-bus capacitor in the system.

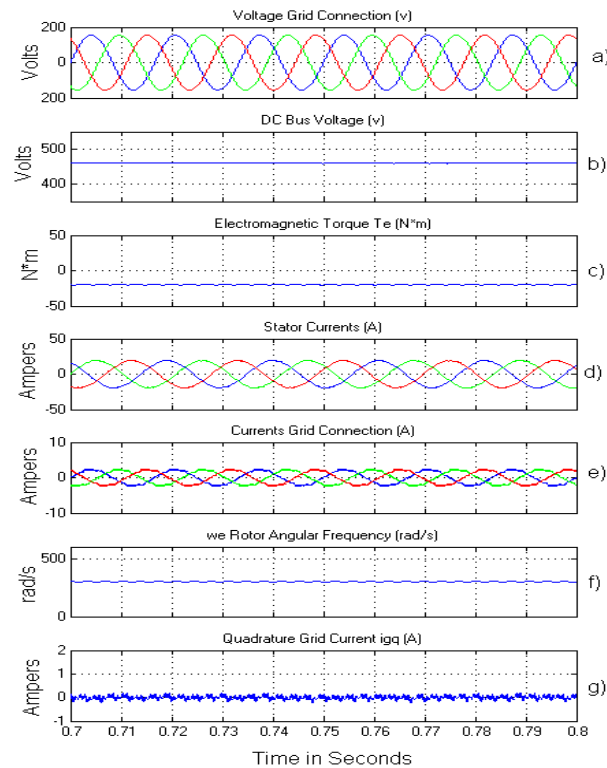


Fig. 8.6 Three-Phase grid connection DC Link capacitor $500\mu\text{F}$ without algorithm

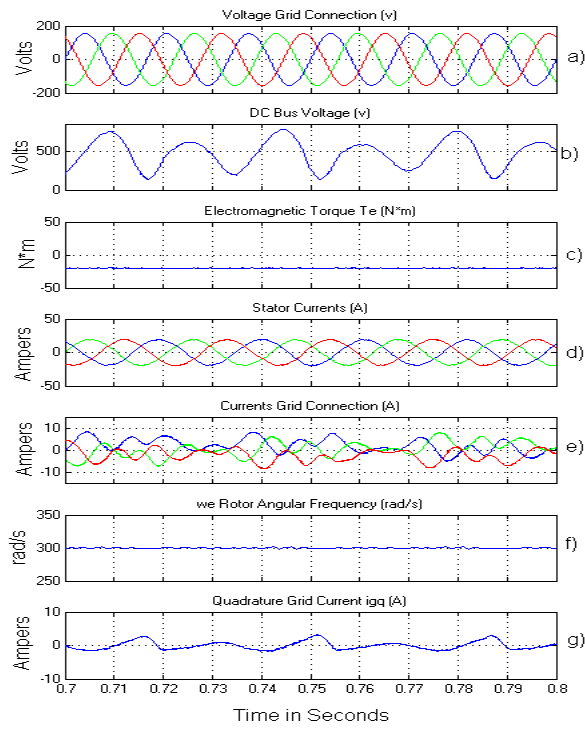


Fig. 8.7 Three-Phase grid connection DC Link capacitor $35\mu\text{F}$ without algorithm

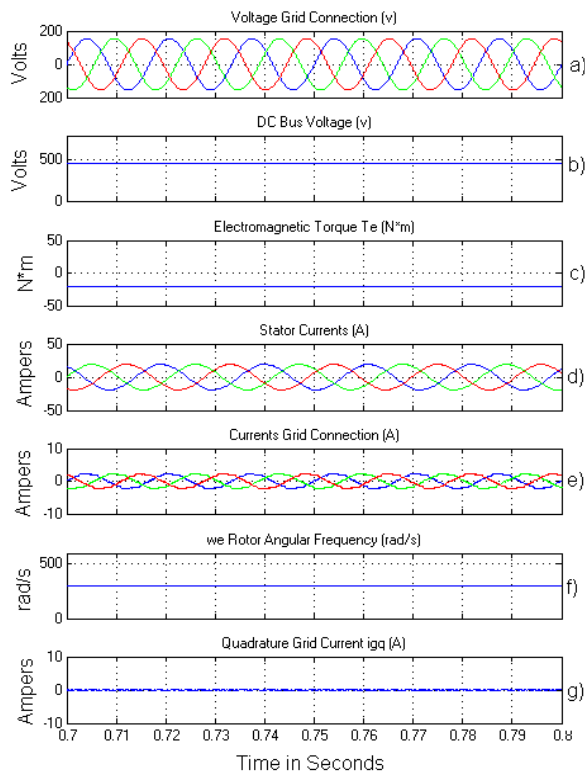


Fig. 8.8 Three-Phase grid connection DC Link capacitor $35\mu\text{F}$ with algorithm

8.4.2 Connection to Single Phase Grid

On the plot shown in (Fig.8.9.a) the frequency of single phase grid voltage is 60Hz. A large capacitor $990\mu\text{F}$ is installed on DC Link. The harmonics on currents and torque are suppressed due to the large DC-Link Capacitance.

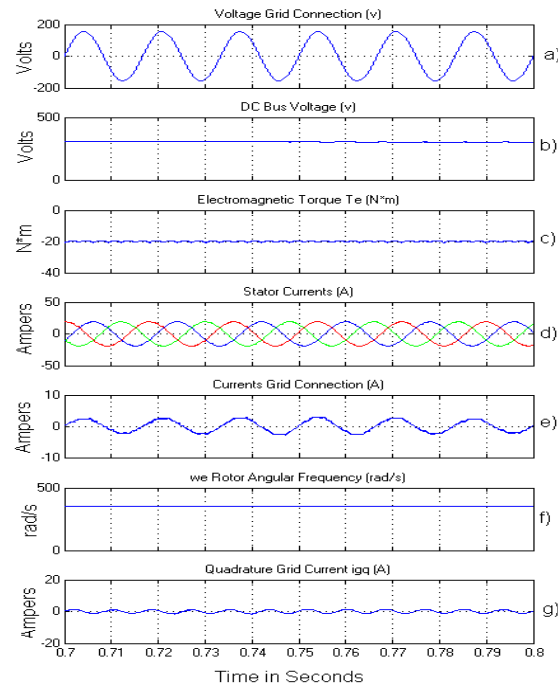


Fig. 8.9 Single-Phase grid connection DC Link capacitor $990\mu\text{F}$ without algorithm

The capacitor is reduced to $60\mu\text{F}$ in order to make the system reliable, but significant ripple components are present in the DC-bus voltage, the torque is pulsating and the stator current is distorted as can be seen from Fig.8.10.

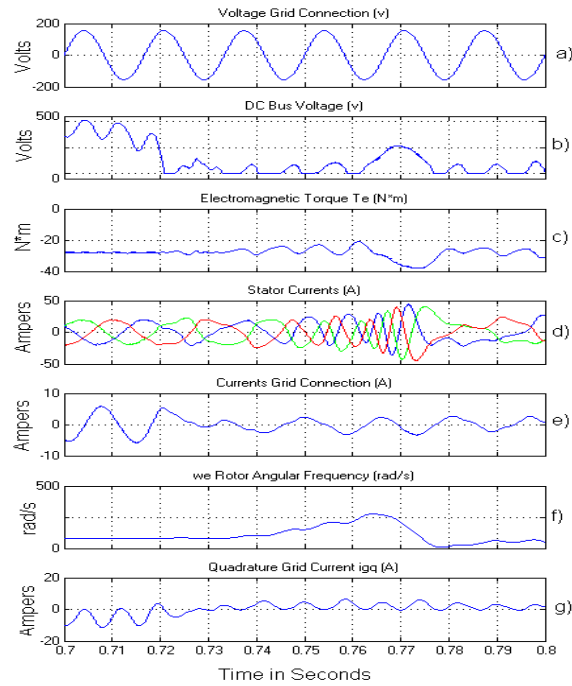


Fig. 8.10 Single Phase grid connection DC Link capacitor $60\mu\text{F}$ without algorithm

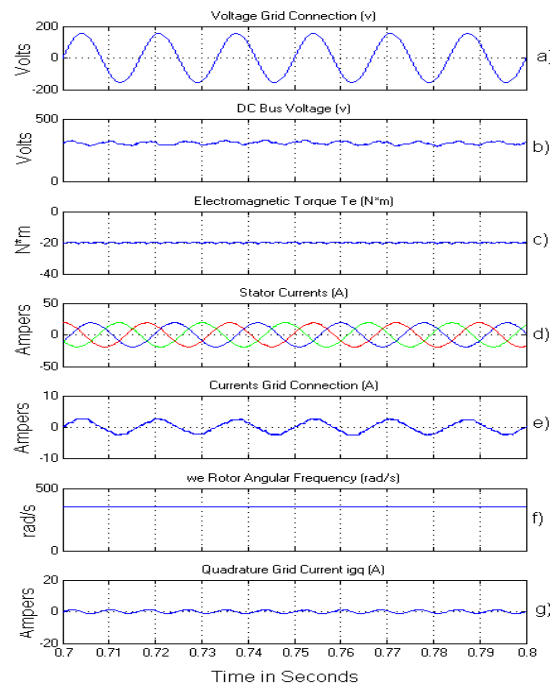


Fig. 8.11 Single Phase grid connection DC Link capacitor $60\mu\text{F}$ with algorithm

Now the small capacitor is conserved on DC Link and the algorithm represented by equation (8.11) is implemented as shown in Fig.8.4 and Fig.8.5.

The waveforms in Fig. 8.11 are for the case when the DC link capacitor is smaller and the proposed algorithm is in effect. It can be seen that the stator currents are undistorted and sinusoidal. The resulting torque is also constant.

8.5 Conclusion

A PMSG wind turbine was connected to a Three-Phase and Single-Phase grid through a back to back converter; with capacitance reduction on DC-Link. Simulations results prove that the proposed algorithm was able to maintain the electromagnetic torque, grid and stator currents without any harmonic frequency due to capacitance reduction.

The shaft of the machine rotates at a frequency which is lower compared to the grid frequency; thus there are no DC components injected in the stator currents, avoiding core saturation.

When the DC Link capacitance is reduced, a ripple component at twice the grid frequency appears in the DC Link, in the case of Single-Phase grid connection. In the case of Three-Phase grid connection the low frequency noise components are introduced. Those frequencies results in a variation of V_{dc} and in the output current on the GSC. The proposed implementation is able to cancel any frequency on DC-Link, because it takes the error information from the same source to be corrected, V_{dc} . With the only fundamental frequency current in the stator, there is no ripple on electromagnetic torque, neither pulsating torque.

A single solution for capacitance reduction is presented in this work. This system is reliable, economical, smaller and, stable.

IX. Final Considerations

The principal aim of this thesis was to present solutions to important issues on two of the most used rotating machines when connected to power converters. Theory of overvoltage on induction machines and mitigation of partial discharges were analyzed with their solutions. The second rotating machine was a permanent magnet synchronous generator connected to the grid through a back to back converter. The related issues and concerns were presented and an innovative control was proposed as a solution.

The overvoltage phenomenon in induction motors connected to inverters has two principal reasons. One of them is when an incident pulse wave from the inverter travels along a cable will behave in well-defined ways at the end of the cable. When there is a mismatch between the cable characteristic surge impedance and the surge impedance of the induction motor, the reflection occurs. This reflection effect of the pulse could be twice the DC bus voltage on the machine terminals. A combination of short rise time and long cable is potentially hazardous for electrical rotating machine insulation. The rise time of the drive pulse primarily determines the critical cable length from the inverter to the motor in order to prevent overvoltage. While the leads between rotating machine and converter is longer, the most high will be the overvoltage on the machine terminals.

To accomplish accurate simulations and laboratory experiments it is necessary to use adequate models of every component. One important step in this thesis was the study of this aspect. The universal induction motor model is an important component in the simulation. It is an extension of the classic T model of induction machine from IEEE 112. The capacitive elements coupling the stator windings, the frame and the rotor are not irrelevant in this case since the voltage feeding the winding has a very high rise time. The new universal motor model is built to predict the behaviour of the motor from low to high frequency. This new model is built from measurements from two induction machines, the first one 75kW and the second was 1.1kW. The machines and the analyser used for the measurements were provided from a local company which was in collaboration with the research for the respective publication of the paper. The measurements in differential mode are with two motor phase terminals linked together as one connector to the analyser and the other as the second connector. To validate the construction of the universal motor model, experimental measurement has been derived and the comparison between the experimental data and simulation data was presented. A simulation was modeled using distributed parameters cable with the measurements accomplished on the laboratory and the induction motor of 1.1kW was used. The same parameters of components from measurements were placed on the simulation. Also the inverter was simulated with the same rise time of the one available on the laboratory. In this case it is a TOPVERT E1 manufactured by TOPTEK ELECTRONICS CORP, with 150 ns of rise time and the DC-Bus voltage was 312V. The cable was 11 AWG 4-conductors PVC Flexible, 7.7 meters long. After run the simulation and the setup on laboratory under the same conditions the accuracy of the motor model was verified being a 2.2% of error on the overvoltage between both results. The slightly error is due to the distributed parameter line model, used for the cable simulation which does not represent parameters of real power lines as for the skin effect. As a conclusion the universal motor model is accurate for the study of overvoltage phenomenon.

The advantage of distributed line parameters over the lumped parameter model is that it provides accurate results in the study of high frequency transients than lumped parameters model. The lumped parameter model cable is calculated from short to open circuit impedances over broad range of frequency. The cable model series parameters are associated to the behavior of the short circuit impedance, while the parallel parameters are associated to the behavior of the open circuit impedances. According to those consideration the lumped parameters model was used on the second case study for the online partial discharge test,

while on the first case study was considerate to use the distributed line parameters. Both cable model have advantages and disadvantages, where in this thesis were shown in order to considerate on every application. In the case of both mentioned case studies cable on laboratory were measured in order to obtain the parameters for their respective simulations.

To obtain the parameters of cable to be applied to the models there are two ways. The first is taking the measurements with a costly RLC bridge, and the second is use a line model on two dimensions in finite element analysis simulation. Therefore the finite element analysis has a disadvantage to be not 100% exactly on parameters results. This is because this method does not considerate the twisted geometry cable situation, which in a real measurements with an RLC bridge does. The advantage of the finite element analysis is that is cheaper, with free student version software. Beside of that during the research accomplished on this thesis were available several RLC bridges and analyzers, and because of the exactitude of measures this method was used.

By definition partial discharge inception voltage is the lowest voltage that is present on insulation machine when the partial discharge occurs. Thus this thesis states that there is a relationship between the overvoltage and the partial discharge activity. Then the solutions available to mitigate the overvoltage on machines showed on case study 1 are also applicable to reduce the partial discharge activity on case study 2. In this thesis two kind of the cheaper filter were analysed. In the case of case study 1 the overvoltage was strongly reduced by a RC terminals machine first order filter. And in the case study 2 the partial discharge inception voltage was mitigated using and LRC filter on the terminals of the inverter. According to the simulation results on case study 1 the overvoltage was reduced from 80% of DC bus to 8% of the DC bus. Other overvoltage factors for different cable lengths were presented without filter. From 15 meters and over, according to Fig. 5.1 the overvoltage factor is twice the DC bus value. Thus the electrical insulation of the machine is under electrical stress, every time a pulse occurs, and possibly causing severe damages to it.

An on line partial discharge test technique on rotating machines fed by inverters was analyzed in this thesis. All the research to determine the configuration of the components was developed using simulation in Matlab SimulinkTM. When overvoltage is present at the machine terminal, electrical stress in the inter-turn insulation and core insulation is also present; this causes aging of the general machine insulation, increasing the dielectric loss and causing partial discharge. If partial discharge occurs at high repetitive rate, it becomes a total

destruction of the insulation, damaging and taking out of service the rotating machine, increasing the cost of operation of the plant. On-line partial discharge testing has a strong advantage upon offline partial discharge test, in on line mode is possible to test the machines without taking them out of service, which can create an economic impact due to interrupted production. With this plan it is possible to avoid the total destruction on the insulation and windings. The online partial discharge measurement technique used in this thesis is based on a coupling capacitor sensor in series with a resistor connected to ground on a filter that suppresses the electrical noise from the power system. The capacitor has a voltage exceeding the expected applied impulse voltage, because it is connected to the machine terminals. The measurement is read by an oscilloscope or an analyzer connected in parallel with a resistor in series with the partial discharge sensor. The coupling capacitor blocks the power frequency 60Hz, while serving as a low-impedance path for the high-frequency partial discharge pulses. The motor model used in this on line partial discharge test, was the 100HP universal induction motor model, and the cable was lumped parameters. In fact the partial discharge was not simulated, but the partial discharge inception voltage, which is defined according to every motor condition. As a simulation result in the first stage the overvoltage was 70% over the DC bus. And the partial discharge impulse inception were placed at the same time when the over voltages were placed. This fact verifies the direct relationship between them. A reactor inverter output second order low-pass LRC Filter was connected between the inverter and cable, thus the rise time was prolonged, and the overvoltage is reduced from 70% to 15% of DC bus. Also plots of partial discharge inception voltage showed a reduction from 5561mV to 708mV.

During the study of issues on Permanent Magnet Synchronous Generator (PMSG) when are connected to the grid through a back to back converter, harmonics on currents and torque where observed. An innovative control was proposed to lead the solution. Due to the success of this new control, a reduction of capacitance on DC link was developed. The content of third paper during the development of this thesis was show on case study 3. There were some ripple present on electro-mechanic torque and currents on grid side converter due to the commutation of switches. The no constant electro-mechanic torque leads to pulsating torque, which the problem is turning in to a mechanical stress on the machine. The use of big capacitance in DC link on back to back converters has the disadvantages of being bulky, expensive, unstable, and unreliable. Those big capacitors also contribute in increasing the response time, cost and losses. The enhanced control consists of modifying the switching

function of the grid side converter. The technique can be applied to three-phase and single-phase DC-AC converters. When there are noise frequencies on the DC Link, it is possible to add that frequencies noise to the switching function, giving a *modified switching function*. With the information of DC-Link error the switching function is modified. When the DC-link voltage differs from the reference value, the switching function is modified; thus compensating the error. In this kind of control where V_{dc} is controlled by grid side converter the error on V_{dc} is corrected. Thus the DC link capacitance can be reduced because there is no more quest of buffer the active power to make V_{dc} constant. Also the ripple from commutation is considered on this error signal and compensated on the *modified switching function*. On simulation results when the system is connected to a three-phase grid, the original DC link capacitor is $500\mu\text{F}$. The high value of capacitance on DC Link is helping, to maintain the DC-Link voltage V_{dc} constant and ripple free. The capacitance is reduced to $35\mu\text{F}$. The DC-Link voltage shows a significant low frequency ripple component. And also as a consequence the stator currents are distorted. When the switching function is modified by the proposed algorithm, the stator currents are undistorted and the DC-bus voltage is ripple free even with a $35\mu\text{F}$ DC-bus capacitor in the system. On simulation results when the system is connected to a single-phase grid, the classic control suggests a DC link capacitor of $990\mu\text{F}$. The capacitor is reduced to $60\mu\text{F}$ in order to make the system reliable, but significant ripple components are present in the DC-bus voltage, the torque is pulsating and the stator current is distorted. The small capacitor was conserved on DC Link and the algorithm is implemented. The DC link voltage and resulting torque are back to be constant and the stator currents are undistorted and sinusoidal.

Issues on the PMSG and induction motors connected to power converters are exposed on this thesis. Every phenomenon on each of the cases was analyzed carefully in order to understand the roots of the problems. After the study of the inconvenient of every case, the solutions were developed in a research accomplished based on theoretical and experimental activities. According to the experimental results the innovative solutions have been satisfied the requirements. Every case of study exposed on this thesis was presented on papers of IEEE conferences by the current author. And the paper on case study 2 is currently on revision to be part of IEEE Industrial Application Society Transaction.

X. Appendix

10.1 Appendix A Parameters of Case Study 3

The numerical values used in control design and in numerical simulations are reported below:

The Grid Side Converter control parameters, connected to the Three-Phase grid, are presented on Table 10.1.

TABLE 10.1
CONTROL PARAMETERS THREE-PHASE CONNECTION

DC-Link voltage (V)	460
DC-Link PID Regulator Kp	0.1
DC-Link PID Regulator Ki	5
DC-Link PID Regulator Kd	0.0001
Current q-d PI Regulator Kp	50
Current q-d PI Regulator Ki	1500
Algorithm k factor	0.6
Inverter Output Inductance Lg(mH)	30
Inverter Output Resistance Rg (Ω)	0.01

The Grid Side Converter control parameters, connected to the Single-Phase grid, are presented on Table 10.2.

TABLE 10.2
CONTROL PARAMETERS SINGLE-PHASE CONNECTION

DC-Link voltage (V)	300
DC-Link PID Regulator Kp	0.0215
DC-Link PID Regulator Ki	0.07
DC-Link PID Regulator Kd	0.0001
Current q-d PI Regulator Kp	1
Current q-d PI Regulator Ki	2000
Algorithm k factor	0.71
Inverter Output Inductance Lg(mH)	30
Inverter Output Resistance Rg (Ω)	0.1
Inverter Output Capacitance Cg (μ F)	10

10.2 Appendix B Clark and Park Transform

Through the use of the Clarke transform, the real (I_d) and imaginary (I_q) currents can be identified. The Park transform can be used to realize the transformation of the I_d and the I_q currents from the stationary to the moving reference frame and control the spatial relationship between the stator vector current and rotor flux vector.

The Clarke transform uses three-phase currents i_a , i_b and i_c to calculate currents in the two-phase orthogonal stator axis: i_α and i_β calculated by the motor flux model, are used to. These two currents in the fixed coordinate stator phase are transformed to the i_d and i_q currents components in the d,q frame with the Park transform.

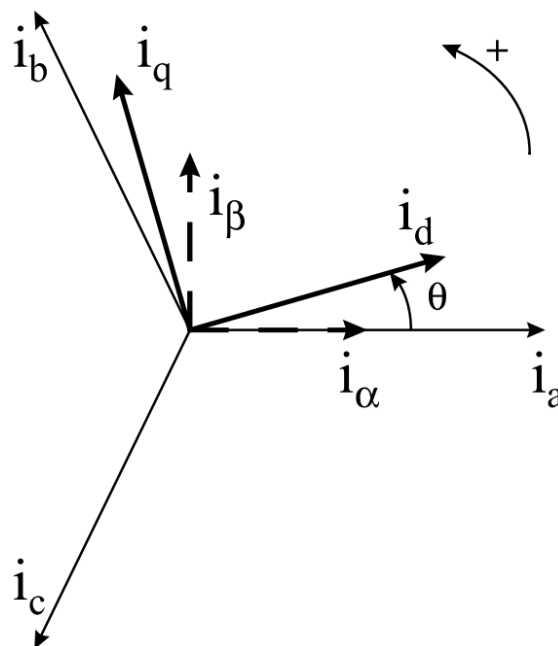


Fig. 10.1 Stator current in the d,q rotating reference frame and its relationship with the a,b and c stationary reference frame

10.2.1 Clark Transform

The mathematical transformation called Clarke transform modifies a three- phase system to a two-phase orthogonal system:

$$i_{\alpha} = \frac{2}{3} * ia - \frac{1}{3}(ib - ic) \quad (10.1)$$

$$i_{\beta} = \frac{2}{\sqrt{3}} * (ib - ic) \quad (10.2)$$

$$i_0 = \frac{2}{3} * (ia + ib + ic) \quad (10.3)$$

Consider now a particular case with i_{α} superposed with i_a and $i_a + i_b + i_c$ is zero, in this condition i_a , i_b and i_c can be transformed to i_{α} and i_{β} with following mathematical transformation:

$$i_{\alpha} = i_a \quad (10.4)$$

$$i_{\beta} = \frac{1}{\sqrt{3}} * i_a + \frac{1}{\sqrt{3}} * ib \quad (10.5)$$

$$i_a + i_b + i_c = 0 \quad (10.6)$$

10.2.2 Park Transform

The two phases α , β frame representation calculated with the Clarke transform is then fed to a vector rotation block where it is rotated over an angle θ to follow the frame d,q attached to the rotor flux.

The rotation over an angle θ is done according to the formulas:

$$i_{sd} = i_{\alpha} \cos(\theta) + i_{\beta} \sin(\theta) \quad (10.7)$$

$$i_{sq} = -i_{\alpha} \sin(\theta) + i_{\beta} \cos(\theta) \quad (10.8)$$

10.2.3 Inverse Park and Clarke Transform

The vector in the d,q frame is transformed from d,q frame to the two phases α , β frame representation calculated with a rotation over an angle θ according to the formulas:

$$i_{\alpha} = i_{sd} \cos(\theta) + i_{sq} \sin(\theta) \quad (10.9)$$

$$i_{\beta} = i_{sd} \sin(\theta) + i_{sq} \cos(\theta) \quad (10.10)$$

The modification from a two phase orthogonal α , β frame to a three-phase system is done by the following equations:

$$i_a = i_{\alpha} \quad (10.11)$$

$$i_b = \frac{1}{2} * i_{\alpha} + \frac{\sqrt{3}}{2} * i_{\beta} \quad (10.12)$$

$$i_c = -\frac{1}{2} * i_{\alpha} + \frac{\sqrt{3}}{2} * i_{\beta} \quad (10.13)$$

10.2.4 Summary

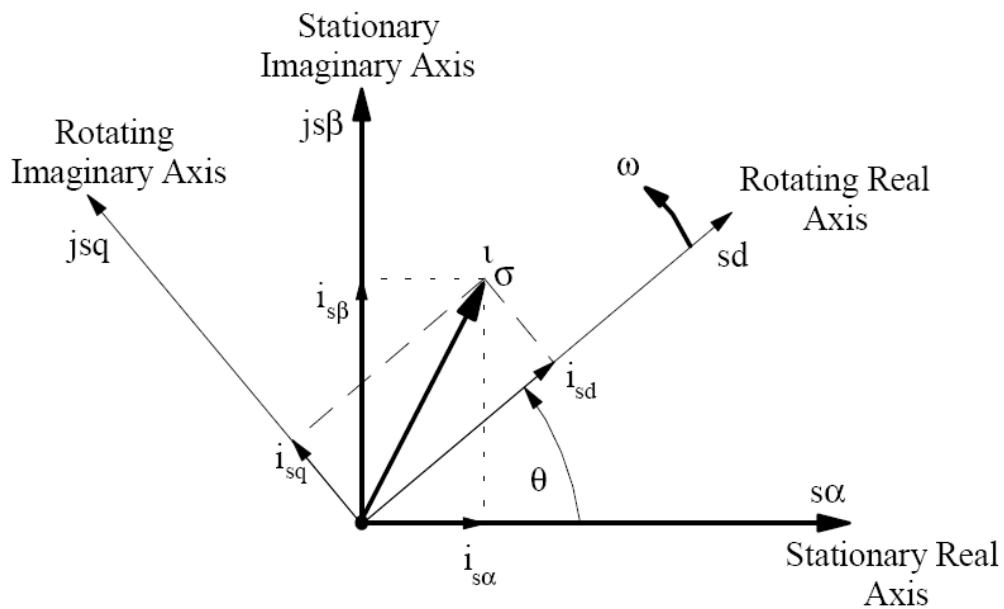


Fig. 10.2 Relationship of current space vector components in stationary and rotating reference frames

10.2.5 Single Phase d-q Transformation

The transformation to the synchronous frame d-q requires two orthogonal components. In three-phase systems the abc components are transformed to the orthogonal and stationary frame system and then to the synchronous frame d-q. However this transformation cannot be applied directly in the single-phase systems, because there is only one variable. This drawback can be solved creating a fictitious input current [60].

It is possible to create a second reference current in quadrature and delayed in relation with i_s , using the same ωt signal. These reference currents are equivalents to the currents in the α , β frame as show in equations [61] below.

$$i_\alpha = i_s = \hat{I} * \cos(\omega t) \quad (10.14)$$

$$i_\beta = \hat{I} * \sin(\omega t) \quad (10.15)$$

$$\begin{bmatrix} i_\alpha \\ i_\beta \end{bmatrix} = \begin{bmatrix} i_L(\omega t + \varphi) \\ i_L(\omega t + \varphi + \pi/2) \end{bmatrix} \quad (10.16)$$

The equivalent d-q frame representation of single phase system and can be represented as:

$$\begin{bmatrix} i_d \\ i_q \end{bmatrix} = \begin{bmatrix} \cos(\theta) & \sin(\theta) \\ -\sin(\theta) & \cos(\theta) \end{bmatrix} * \begin{bmatrix} i_\alpha \\ i_\beta \end{bmatrix} \quad (10.17)$$

XI. References

- [1] A. Narang, B. Gupta, E. Dick, and D. Sharma, "Measurement and analysis of surge distribution in motor stator windings," *IEEE Transactions on Energy Conversion*, vol. 4, no. 1, pp. 126-134, 1989.
- [2] C. Hudon, N. Amyot, T. Lebey, P. Castelan, and N. Kandeov, "Testing of Low-voltage Motor Turn Insulation Intended for Pulse-width Modulated Applications," *IEEE Transactions on Dielectrics and Electrical Insulation*, vol. 7, no. 6, pp. 783-789, 2000.
- [3] S. Bell and J. Sung, "Will your motor insulation survive a new adjustable-frequency drive?," *IEEE Transactions on Industry Applications*, vol. 33, no. 5, pp. 1307-1311, 1997.
- [4] L. a. Saunders, G. L. Skibinski, S. T. Evon, and D. L. Kempkes, "Riding the reflected wave-IGBT drive technology demands new motor and cable considerations," *Proceedings of 1996 IAS Petroleum and Chemical Industry Technical Conference*, pp. 75-84, 1996.
- [5] L. Palma and P. Enjeti, "An inverter output filter to mitigate dV/dt effects in PWM drive system," *APEC. Seventeenth Annual IEEE Applied Power Electronics Conference and Exposition (Cat. No.02CH37335)*, vol. 0, no. c, pp. 550-556, 2002.
- [6] H. De Paula, D. A. D. Andrade, M. L. R. Chaves, J. L. Domingos, and M. A. A. de Freitas, "Methodology for Cable Modeling and Simulation for High-Frequency Phenomena Studies in PWM Motor Drives," *IEEE Transactions on Power Electronics*, vol. 23, no. 2, pp. 744-752, Mar. 2008.
- [7] G. Gao and W. Chen, "Design Considerations and Qualifications of the Insulation System for Double Fed Induction Wind Generator," *Iris Rotating Machine Conference*, no. June, pp. 1-4, 2007.
- [8] F. Castelli Dezza, M. M. Maglio, G. Marchegiani, D. F. Ortega, and D. Rosati, "Reduction of Motor Overvoltage fed by PWM AC Drives using a Universal Model," in *XIX International Conference on Electrical Machines - ICEM 2010, Rome, 2010*, pp. 0-5.
- [9] IEEE, *IEEE Trial-Use Guide to the Measurement of Partial Discharges in Rotating Machines*. New York, NY 10016-5997, USA: , 2000.
- [10] CEI, "CEI, IEC Technical Specification TS 60034-18-41 first edition 2006-10." 2006.
- [11] I. Blokhintsev, B. J. Cassidy, C. L. Patterson, and A. H. Loesch, "Advantage of On-Line Partial Discharge Continuous Monitoring of Medium Voltage Substation," *Spectrum*, no. June, pp. 153-158, 2009.
- [12] D. F. Ortega and F. Castelli Dezza, "On line Partial Discharges Test on Rotating Machines Supplied by IFDs," *XIX International Conference on Electrical Machines - ICEM 2010, Rome*, pp. 4-7, 2010.

-
- [13] M. Chapman and R. Bruetsch, "Suppression of Partial Discharges in High-Voltage Rotating Machines," *IEEE Electrical Insulation Conference*, no. June, pp. 338-342, 2009.
- [14] C. Petrarca, G. Lupo, and L. Egiziano, "Steep Fronted Overvoltages in Inverter Fed Induction Motors Numerical Identification of Critical Parameters," *IEE High Voltage Engineering Symposium*, pp. 433-436, 1999.
- [15] P. Vas, *Electrical Machines and Drives*. Oxford University Press, 1992.
- [16] D. F. Ortega, W. Shireen, and F. Castelli-Dezza, "Control for Grid connected PMSG Wind Turbine with DC Link Capacitance Reduction," in *Power & Energy Society Transmission and Distribution Conference and Exposition*, 2012.
- [17] E. Persson, "Transient effects in application of PWM inverters to induction motors," *IEEE Transactions on Industry Applications*, vol. 28, no. 5, pp. 1095-1101, 1992.
- [18] S.-jun Kim and S.-K. Sul, "A Novel Filter Design for Suppression of High Voltage Gradient in Voltage-Fed PWM Inverter," *Proceedings of APEC 97 - Applied Power Electronics Conference*, vol. 1, pp. 122-127, 1997.
- [19] Y. Jiang, X. Chen, and D. Xu, "Research on a Novel Inverter Output Passive Filter for Reducing dv/dt at Motor Terminals in a PWM Drive System," in *Electrical Machines and Systems, 2003. ICEMS 2003. Sixth International Conference*, 2003, pp. 436-439.
- [20] K. Sander and G. Reed, "Transmission and Propagation of Electromagnetic Waves," Cambridge, 1986.
- [21] A. H. Bonnett, "Analysis of the Impact of Pulse-Width Modulated Inverter Voltage Waveforms on AC Induction Motors," *IEEE Transactions on Industry Applications*, vol. 32, no. 2, 1996.
- [22] R. H. Rehder, "Preliminary evaluation of motor insulation for variable speed applications," *Proceedings of Electrical/Electronics Insulation Conference*, pp. 333-336.
- [23] K. Bultemeier, D. Barta, and D. Floryan, "Dielectric integrity of magnet wire insulations under multi-stresses," *Proceedings:Electrical Electronics Insulation Conference and Electrical Manufacturing & Coil Winding Conference*, pp. 257-261.
- [24] G. Skibinski, "Technical Report on Reflected wave Impact on Motors and Cables," 1995.
- [25] S. Amarir and K. Al-Haddad, "A Modeling Technique to Analyze the Impact of Inverter Supply Voltage and Cable Length on Industrial Motor-Drives," *IEEE Transactions on Power Electronics*, vol. 23, no. 2, pp. 753-762, Mar. 2008.
- [26] J. Adabi, F. Zare, a. Ghosh, and R. D. Lorenz, "Calculations of capacitive couplings in induction generators to analyse shaft voltage," *IET Power Electronics*, vol. 3, no. 3, p. 379, 2010.

-
- [27] B. Mirafzal, G. L. Skibinski, R. M. Tallam, D. W. Schlegel, and R. a. Lukaszewski, "Universal Induction Motor Model With Low-to-High Frequency-Response Characteristics," *IEEE Transactions on Industry Applications*, vol. 43, no. 5, pp. 1233-1246, 2007.
- [28] B. Mirafzal, G. Skibinski, R. Tallam, D. Schlegel, and R. Lukaszewski, "Determination of Parameters in the Universal Induction Motor Model," *IEEE Transactions on Industry Applications*, vol. 45, no. 1, pp. 142-151, Oct. 2009.
- [29] B. Basavaraja and D. V. S. S. S. Sarma, "Modeling and Simulation of dv/dt Filters for AC Drives with Fast Switching Transients," *2006 IEEE Power India Conference*, pp. 654-661, 2006.
- [30] A. Moreira, T. Lipo, G. Venkataramanan, and S. Bernet, "Modeling and Evaluation of dv/dt Filters for AC Drives with High Switching Speed," in *Power Electronics and Applications European Conference*, 2001, pp. 1-14.
- [31] G. Skibinski, R. Tallam, R. Reese, B. Buchholz, and R. Lukaszewski, "Common Mode and Differential Mode Analysis of Three Phase Cables for PWM AC Drives," *Conference Record of the 2006 IEEE Industry Applications Conference Forty-First IAS Annual Meeting*, vol. 0, no. c, pp. 880-888, Oct. 2006.
- [32] A. Corporation, "Maxwell 2D Ver. 9 and Simplorer." 2002.
- [33] Matworks, "Matlab Simulink." 2011.
- [34] G. Skibinski, J. Erdman, J. Pankau, and J. Campbell, "Assessing AC motor dielectric withstand capability to reflected voltage stress using corona testing," in *Industry Applications Thirty First IAS Conference*, 1996, pp. 694-702.
- [35] R. J. Kerkman, D. Leggate, and G. L. Skibinski, "Interaction of drive modulation and cable parameters on AC motor transients," *IEEE Transactions on Industry Applications*, vol. 33, no. 3, pp. 722-731, 1997.
- [36] M. Melfi, A. Sung, S. Bell, and G. Skibinski, "Effect of surge voltage risetime on the insulation of low-voltage machines fed by PWM converters," *IEEE Transactions on Industry Applications*, vol. 34, no. 4, pp. 766-775, 1998.
- [37] H.-jong Kim, G.-ho Lee, C.-ho Jang, and J.-pil Lee, "Cost-effective design of an inverter output reactor in ASD applications," *IEEE Transactions on Industrial Electronics*, vol. 48, no. 6, pp. 1128-1135, 2001.
- [38] A. von Jouanne, P. Enjeti, and W. Gray, "Application Issues for PWM Adjustable Speed AC Motor Drives," *IEEE Industry Applications Magazine*, 1996.
- [39] G. Skibinski, "Design Methology of a Cable Terminator to Reduce Reflected Voltage on AC motors," *IEEE Transactions on Industry Applications*, 1996.

- [40] M. Hongfei and X. Dianguo, "Research of Inverter Output Filters for PWM Drives," in *Electrical Machines and Systems, 2001. ICEMS 2001. Proceedings of the Fifth International Conference on*, 2001.
- [41] S. Walter, "Inverter Output Filter Effect on PWM Motor Drives of a Flywheel Energy Storage System," *2nd International Energy Conversion Engineering Conference NASA Center for Aerospace Information*, no. September, 2004.
- [42] J. Yanshu, X. Dianguo, and C. Xiyu, "A Novel Inverter Output dv/dt Suppression Filter," in *Industrial Electronics Society, 2003. IECON '03. The 29th Annual Conference of the IEEE*, 2003, pp. 2901-2905.
- [43] A. von Jouanne and P. N. Enjeti, "Design considerations for an inverter output filter to mitigate the effects of long motor leads in ASD applications," *IEEE Transactions on Industry Applications*, vol. 33, no. 5, pp. 1138-1145, 1997.
- [44] D. Leggate, J. Pankau, D. W. Schlegel, R. J. Kerkman, and G. L. Skibinski, "Reflected waves and their associated current," *IEEE Transactions on Industry Applications*, vol. 35, no. 6, pp. 1383-1392, 1999.
- [45] F. Moreira, T. Lipo, G. Venkataramanan, and S. Bernet, "High-frequency modeling for cable and induction motor overvoltage studies in long cable drives," *IEEE Transactions on Industry Applications*, vol. 38, no. 5, pp. 1297-1306, Sep. 2002.
- [46] www.newtons4th.com, "Newtons4th Ltd. model PSM1735 Frequency Response Analyzer 10 μ Hz-35MHz," 2009. [Online]. Available: <http://www.ncbi.nlm.nih.gov/pubmed/10768541>.
- [47] H. Kim, T. M. Jahns, and G. Venkataramanan, "Minimization of reverse recovery effects in hard-switched inverters using CoolMOS power switches," *Conference Record of the 2001 IEEE Industry Applications Conference. 36th IAS Annual Meeting (Cat. No.01CH37248)*, vol. 0, no. C, pp. 641-647, 2001.
- [48] G. C. Stone, S. R. Campbell, and M. Susnik, "New tools to determine the vulnerability of stator windings to voltage surges from IFDs," *Proceedings: Electrical Insulation Conference and Electrical Manufacturing and Coil Winding Conference (Cat. No.99CH37035)*, pp. 149-153.
- [49] H. Zhu, V. Green, and M. Sasic, "Development of High Sensitivity Capacitors for PD Measurement in Operating Motors and Generators," *Proceedings of the 6th International Conference on Properties and Applications of Dielectric Materials*, pp. 571-574, 1999.
- [50] G. Stone, E. Boulter, and I. Culbert, *Electrical Insulations for Rotating Machines*, vol. 20, no. 3. 2004, pp. 195-209.
- [51] M. Tozzi, G. Montanari, D. Fabiani, and A. Cavallini, "Off-Line and On-Line PD Measurements on Induction Motors Fed by Power Electronic Impulses," *IEEE Electrical Insulation Conference*, no. June, pp. 420-424, 2009.

-
- [52] and J. C. B. Monica Chinchilla, Santiago Arnaltes, "Control of Permanent-Magnet Generators Applied to Variable-Speed Wind-Energy Systems Connected to the Grid," *IEEE Transactions on Energy Conversion*, vol. 21, no. March, pp. 130-135, 2006.
- [53] G. Utility Wind Integration, "Utility Wind Integration State of the Art," 2006.
- [54] A. Grauers, "Efficiency of three wind energy generator systems," *IEEE Transactions on Energy Conversion*, vol. 11, no. 3, pp. 650-657, 1996.
- [55] A. Shamsnia, H. Hojabri, and H. Mokhtari, "A New Control Method of Three-Phase PMSG Wind Turbine Connected to Single-Phase Network Through a Back-to-Back Converter," *IEEE Industry Applications Magazine*, vol. 2, no. 2, pp. 2-5, 2011.
- [56] F. S. dos Reis, S. Islam, K. Tan, J. V. Ale, F. D. Adegas, and R. Tonkoski, "Harmonic Mitigation in Wind Turbine Energy Conversion Systems," in *IEEE Power Electronics Specialists Conference*, 2006, no. 2, pp. 1-7.
- [57] S. H. Kaboli, M. R. Zolghadri, and A. Homaifar, "Effects of sampling time on the performance of direct torque controlled induction motor drive," in *IEEE International Symposium on Industrial Electronics*, 2003, vol. 2, no. 4, pp. 1049-1052.
- [58] W. Shireen, A. Nagarajan, and S. Patel, "A Reliable Low Cost Power Electronics Interface for Photovoltaic Energy Systems using a Single DSP Controller," *IEEE Power System Conference 2011 Arizona*, pp. 1-6.
- [59] P. N. Enjeti and W. Shireen, "A New Technique to Reject DC-Link Voltage Ripple for Inverters Operating on Programmed PWM Waveforms," *IEEE Transactions on Power Electronics*, vol. 7, no. 1, pp. 171-180, 1992.
- [60] U. A. Miranda, M. Aredes, and L. Rolim, "A DQ Synchronous Reference Frame Control for Single-Phase Converters," in *Power Electronis Specialist*, 2005, pp. 1377-1381.
- [61] V. Khadkikar, M. Singh, A. Chandra, and B. Singh, "Implementation of Single-phase Synchronous d- q Reference Frame Controller for Shunt Active Filter under Distorted Voltage Condition," in *Power Electronics and Drives Energy Systems*, 2010, pp. 1-6.